MITSUBISHI ELECTRIC RESEARCH LABORATORIES
http://www.merl.com

A Stochastic Geometry Analysis of Large-scale Cooperative Wireless Networks Powered by Energy Harvesting

Khan, Talha; Orlik, Philip V.; Kim, Kyeong Jin; Heath, Robert W.; Sawa, Kentaro

TR2017-030 January 28, 2017

Abstract

Energy harvesting is an emerging technology for enabling green, sustainable, and autonomous wireless networks. In this paper, a large-scale wireless network with energy harvesting transmitters is considered, where a group of transmitters forms a cluster to cooperatively serve a desired receiver amid interference and noise. To characterize the link-level performance, closed-form expressions are derived for the transmission success probability at a receiver in terms of key parameters such as node densities, energy harvesting parameters, channel parameters, and cluster size, for a given cluster geometry. The analysis is further extended to characterize a network-level performance metric, capturing the tradeoff between link quality and the fraction of receivers served. Numerical simulations validate the accuracy of the analytical model. Several useful insights are provided. For example, while more cooperation helps improve the link-level performance, the network-level performance might degrade with the cluster size. Numerical results show that a small cluster size (typically 3 or smaller) optimizes the network-level performance. Furthermore, substantial performance can be extracted with a relatively small energy buffer. Moreover, the utility of having a large energy buffer increases with the energy harvesting rate as well as with the cluster size in sufficiently dense networks.

IEEE Transactions on Communications

A Stochastic Geometry Analysis of Large-scale Cooperative Wireless Networks Powered by Energy Harvesting

Talha Ahmed Khan, *Member, IEEE*, Philip Orlik, *Senior Member, IEEE*, Kyeong Jin Kim, *Senior Member, IEEE*, Robert W. Heath Jr., *Fellow, IEEE*, and Kentaro Sawa

***Abstract*—Energy harvesting is an emerging technology for enabling green, sustainable, and autonomous wireless networks. In this paper, a large-scale wireless network with energy harvesting transmitters is considered, where a group of transmitters forms a cluster to cooperatively serve a desired receiver amid interference and noise. To characterize the link-level performance, closed-form expressions are derived for the transmission success probability at a receiver in terms of key parameters such as node densities, energy harvesting parameters, channel parameters, and cluster size, for a given cluster geometry. The analysis is further extended to characterize a network-level performance metric, capturing the tradeoff between link quality and the fraction of receivers served. Numerical simulations validate the accuracy of the analytical model. Several useful insights are provided. For example, while more cooperation helps improve the link-level performance, the network-level performance might degrade with the cluster size. Numerical results show that a small cluster size (typically 3 or smaller) optimizes the network-level performance. Furthermore, substantial performance can be extracted with a relatively small energy buffer. Moreover, the utility of having a large energy buffer increases with the energy harvesting rate as well as with the cluster size in sufficiently dense networks.**

***Index Terms*—Energy harvesting, stochastic geometry, cooperative wireless networks.**

I. Introduction

ENERGY harvesting is a promising approach for realizing self-powered wireless networks. A wireless device equipped with energy harvesting capability may extract energy from natural or man-made sources such as solar radiations, wind, radio frequency (RF) signals, indoor lighting, etc. [2], [3]. Energy harvesting could potentially transform both infrastructure-based as well as ad hoc wireless networks. For instance, in cellular systems, energy harvesting could help cut the operating expenditures for the cell-sites, reduce the carbon footprint as well as facilitate cell-site deployment [4]. Similarly, energy harvesting is also closely related to the Internet of Things [5], which broadly is a network consisting of everyday objects such as machines, buildings, vehicles, etc. Many of these *smart* objects will contain low-power wireless sensors that communicate with other devices and/or a control unit. Energy harvesting can potentially enhance the battery lifetimes while simplifying the network maintenance (for instance, with an energy harvesting device, no human intervention would be needed for battery replacement), thus providing the much-needed autonomy for sustaining such networks [2], [5], [6].

Energy harvesting devices need new communication protocols. Due to limited energy storage capacity and depending on the type of harvesting, the energy availability at the device varies over time. This leads to a model where energy arrivals are bursty. Several papers have proposed optimal transmission policies assuming causal or non-causal knowledge about energy arrivals for different setups (see [2], [7] for a comprehensive review). For example, a point-point link [8], [9], an interference channel [10], and a broadcast channel [11] have been considered. While prior research has mostly considered simple information-theoretic setups, some recent studies have investigated the network-level dynamics in large *non-cooperative* wireless networks powered by energy harvesting [4], [12]–[14].

Stochastic geometry is emerging as a popular tool for analyzing a variety of setups ranging from ad hoc, to cognitive and cellular networks. It often leads to tractable analytical models that yield general performance insights, thus obviating the need of exhaustive simulations [15]. The performance of ad hoc networks has been characterized using metrics such as outage probability and transmission capacity [16]–[18]. Similar analysis has been applied to single and multi-tier cellular networks under different assumptions about cell association, scheduling and power control [18]–[20]. Multi-cell cooperation has been analyzed for different cooperation models in [21]–[25]. For example, dynamic coordinated beamforming was treated in [21], random clustering with intercell interference nulling was considered in [22], and pairwise cooperation with limited channel knowledge was analyzed in [23]. Similarly, joint transmission without prior channel knowledge and/or tight synchronization has also been considered [24], [25]. None of the aforementioned work [21]–[25] on *cooperative* networks, however, considers energy harvesting.

Stochastic geometry has also been used for analyzing energy harvesting systems. Large-scale self-powered ad hoc networks have been analyzed in [12] and [13]. In [12], the network model consists of a large number of energy harvesting transmitters, where each transmitter has a dedicated receiver

T. A. Khan and R. W. Heath Jr. are with The University of Texas at Austin, Austin, TX, USA (Email: {talhakhan, rheath}@utexas.edu). P. Orlik and K. J. Kim are with Mitsubishi Electric Research Lab (MERL), Cambridge, MA, USA (Email:{porlik, kkim}@merl.com). K. Sawa is with Mitsubishi Electric Corporation IT R&D Center, Kamakura, Kanagawa, Japan (Email: Sawa.Kentaro@bk.MitsubishiElectric.co.jp).

This work was initiated while T. A. Khan was with MERL, and was supported by a gift from MERL.

Parts of this paper were presented at the 2015 IEEE International Conference on Communications [1].

located a fixed distance away. Leveraging tools from stochastic geometry and random walk theory, spatial throughput was derived by optimizing over the transmission power. For a similar setup, the authors in [13] derived the transmission capacity for a random access network by optimizing over the medium access probability. Self-powered heterogeneous cellular networks have been considered in [4]. In [4], base-station availability (i.e., the fraction of the time it can remain ON) was analytically characterized using tools from random walk theory and stochastic geometry. The work in [4], [12] and [13], however, does not consider any node cooperation or joint transmission at the physical layer. Cooperative/joint transmission seems particularly attractive for energy harvesting networks, as it could compensate for the performance loss due to uncertain energy availability at the transmitters.

In another line of work, wireless-powered communication networks have also been investigated using a stochastic geometry framework [14], [26]–[29]. In [14], the performance of a cognitive network with opportunistic wireless energy harvesting was characterized. In [26], a hybrid cellular network consisting of both base-stations and power beacons was proposed to enable wireless power transfer to mobiles. The trade-offs between the deployment densities and transmit power were investigated under an outage constraint on the data links. The work in [27] characterized the performance of wireless information and energy transfer in a millimeter wave cellular network. Similarly, the performance of wireless information and energy transfer in relay-aided networks has also been characterized for various relaying strategies [28], [29]. In this work, however, we do not study wireless information and energy transfer.

In this paper, we consider a large-scale network of transmitters and receivers, where a receiver node is jointly served by a cluster consisting of its K closest self-powered transmitter nodes. This model is attractive for many scenarios involving energy harvesting wireless communications such as self-powered sensor networks, self-powered wireless hotspots, and other IoT-inspired applications of the future [2], [5], [6]. We provide a tractable framework to characterize the system performance as a function of key parameters such as the cluster size, the energy harvesting capability, the transmitter/receiver densities and other network and channel parameters. We model the locations of the transmitters and receivers using independent Poisson point processes (PPPs). To reap the benefits of cooperation, the transmitters are grouped into clusters such that all the in-cluster transmitters jointly serve a common receiver, which is subjected to interference from the out-of-cluster nodes. Channel acquisition and node coordination, which is formidable even for conventional networks, is typically exacerbated with energy harvesting nodes. This motivates us to adopt non-coherent joint transmission as the cooperation model. The performance of such a *cooperative* self-powered wireless network in a stochastic geometry framework has not been analyzed in the literature.

The proposed analytical model captures the key interplay between the cluster size and the transmitter and receiver densities. Note that a transmitter cluster may have multiple candidate receivers, only one of which will be served in a given resource. We therefore consider a performance metric that captures the two key events influencing the overall performance: (i) a receiver is selected for service (modeled via cluster access probability in Section III-B), and (ii) the transmission is successful (modeled via link success probability in Section III-A). For the former, we propose an analytical approximation for the cluster access probability in terms of the cluster size and the ratio of the transmitter and receiver densities. For the latter, we derive simple analytical expressions that characterize the link performance as a function of system parameters (e.g., energy harvesting rate, energy buffer size, transmitter density), channel parameters and cluster geometry, while accounting for the heterogeneous network interference. Leveraging these results (each being a novel contribution in itself), a closed-form analytical expression is derived for the overall performance metric, and validated using simulations.

We also investigate the impact of cluster size, energy harvesting rate and energy buffer size on the overall performance. Our findings suggest that (i) there is an optimal cluster size that maximizes the overall performance given the density parameters; (ii) the optimal cluster size increases with the ratio of transmitter and receiver densities and typically ranges from 1 to 3; (iii) a relatively small energy buffer size (typically large enough to store 10 or fewer transmissions in the considered setup) is sufficient for extracting performance gains; and (iv) the utility of having a large energy buffer increases with the energy harvesting rate as well as with the cluster size when the density ratio is sufficiently large. Our analytical model is applicable to a general class of networks, with the traditionally-powered cooperative and non-cooperative networks as special cases.

This paper is an extension of our previous conference paper [1] where a similar setup was considered. Unlike [1] which only considers the link-level performance, we analytically characterize both the link and network-level performance in this paper while incorporating heterogeneous network interference in our model. The rest of the paper is organized as follows. The system model is described in Section II. Using tools from stochastic geometry, the analytical expressions for the considered performance metrics are derived in Section III. Section IV presents the simulation results and Section V concludes the paper.

II. System Model

We now describe the energy harvesting model, the underlying assumptions about the considered network, and the cooperation scenario.

A. Energy Harvesting Model

We consider a wireless network consisting of transmitters equipped with energy harvesting modules. An energy harvesting module extracts energy from a source and stores it in an energy buffer. For instance, an RF energy harvesting module typically consists of a *rectenna* element that rectifies the received RF signal, which is then used for charging a battery (energy buffer). The energy arrivals at the energy buffer are assumed to be random and independent across nodes. None

of the transmitters are privy to any non-causal information about energy arrivals. We now describe the energy harvesting model for an arbitrary transmitter equipped with an energy buffer of size $S \in \mathbb{N}$. The energy arrives at the buffer with rate ρ following an independent and identically distributed (IID) Bernoulli process[1], i.e., with probability ρ, one unit of energy arrives at the buffer in time-slot t, while $1-\rho$ is the probability that no energy arrives at the buffer in that slot. A node may choose to transmit with fixed power $\tilde{P}$ if it has sufficient energy in the buffer. No power control is assumed, therefore each transmission depletes the buffer of $\tilde{P}$ units of energy. The energy arrivals are modeled using a birth-death Markov process along the lines of [12], [13], [30], [31].

For medium access, we consider a slotted ALOHA based random access protocol where in each time-slot, a node (having sufficient energy) accesses the medium with probability p_{ch} independently of other nodes. Let p_S denote the probability that a node has the requisite amount of energy available in the buffer of size S. Then, $p_S = \Pr\left[A_S(t) \geq \tilde{P}\right]$, where $A_S(t)$ denotes the state (i.e., energy level) of the buffer at time t. We now define p_{tr}, the transmission probability of an arbitrary node, and express it as a function of system parameters.

Lemma 1. For energy arrivals with rate $\rho > 0$, finite energy buffer of size $S \in \mathbb{N}$, and channel access probability $p_{\text{ch}} > 0$, it follows that $p_{\text{tr}} = p_{\text{ch}} p_S$ in steady state, where

$$p_S = \begin{cases} \frac{\rho}{\rho + p_{\text{ch}} - \rho p_{\text{ch}}} & S = 1 \\ \frac{\frac{\rho}{p_{\text{ch}}}\left(1 - \left(\frac{\rho(1-p_{\text{ch}})}{p_{\text{ch}}(1-\rho)}\right)^S\right)}{1 - \frac{\rho}{p_{\text{ch}}}\left(\frac{\rho(1-p_{\text{ch}})}{p_{\text{ch}}(1-\rho)}\right)^S} & S > 1, \rho \neq p_{\text{ch}} \\ \frac{S}{S+1-\rho} & S > 1, \rho = p_{\text{ch}} \end{cases} \quad (1)$$

for the case $\tilde{P} = 1$.

Proof. It can be proved by solving the balance equations for the resulting Markov chain (e.g., see [12]). ■

Note that $0 < p_{\text{tr}} \leq p_{\text{ch}}$ since $\lim_{\rho \to 1} p_{\text{tr}} = p_{\text{ch}}$, where $\rho = 1$ corresponds to the case when the node is powered by conventional power sources. Furthermore, p_{ch} is fixed throughout the network. Therefore, the transmission probability of a node varies as a function of the energy harvesting rate and buffer size. In other words, the higher the p_{tr} of a node, the more superior the energy harvesting capability (i.e., harvesting rate and/or buffer size). Note that Lemma 1 has been specialized for the case $\tilde{P} = 1$, which is consistent with the system model explained in the next section. This is because, without loss of generality, we will consider an equivalent system where the transmit power of each node is normalized with respect to that of a reference node, and the reference node uses a unit transmit power (see the discussion following equation (3) for details). Moreover, the reference transmitter with a full buffer can transmit for S slots without requiring recharging.

[1] Due to analytical tractability, this is a common approach for modeling an energy harvesting process (e.g., see [13], [30], [31]). Conceptually, the energy harvesting rate in this model approximates the average energy arrival rate of an actual (continuous) energy harvesting process. With RF energy harvesting, for example, the energy arrivals will randomly fluctuate across slots. When the received energy exceeds a certain threshold, it may be regarded as an energy arrival in the buffer. Otherwise, we may assume that no energy arrived in the buffer in that slot.

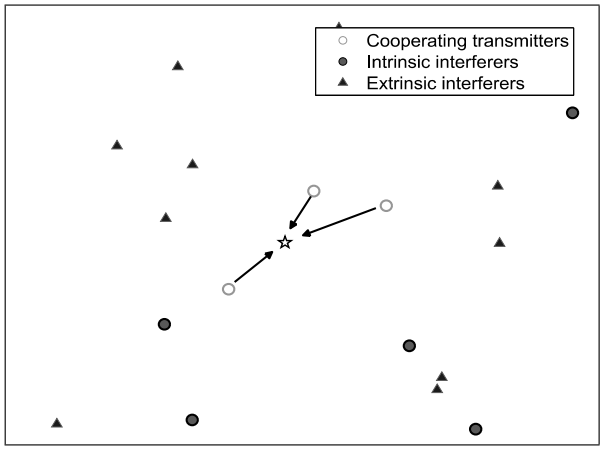

Fig. 1. A network snapshot showing a receiver (☆) jointly served by a cluster of $K = 3$ closest transmitters amid intrinsic and extrinsic interference. Only one receiver is shown for illustration purpose.

B. Network Model

We consider a large-scale network consisting of transmitters (TXs) and receivers (RXs) where the TX locations are drawn from a homogeneous PPP of intensity (density) λ, which we denote as $\Phi \triangleq \{x_i, i \in \mathbb{N}\}$. Similarly, the RX (or user) locations are modeled using another PPP Φ_u of intensity λ_u, which is assumed to be independent of Φ. In the considered setup, a cluster of K (self-powered) cooperating TXs jointly serves a desired RX over the same time-frequency resource block. We assume that each RX is served by its K closest TXs in Φ (see Fig. 1). When there are multiple candidate users competing over one or more TXs of a potential cluster, we assume that only one user will be selected for service (uniformly at random) in each time-slot (see Section III-B). This cluster association will possibly entail some control signaling between the transmitters and users. For example, the transmitters may transmit a periodic control beacon to facilitate the users in identifying their closest transmitters. The users may then request access to their desired set of transmitters. Since the control signaling phase will usually be much smaller than the data transmission phase, we focus on the latter in this paper. We further assume that the TXs in Φ are active with a transmission probability p_{tr} (Lemma 1, Section II-A). For example, when a TX has no candidate user in Φ_u (i.e., void cell), it may still transmit to (wirelessly) charge other inactive users, or to serve other opportunistic users in the network (performance characterization of such users, though, is not the focus of this work).

Consider an arbitrary user in Φ_u being jointly served by a cluster consisting of its K closest TXs in Φ. It suffers from co-channel interference due to concurrent transmissions from the out-of-cluster nodes in Φ. We call the interference originating from Φ as *in-network* or *intrinsic* interference. Note that the user may receive additional interference from other out-of-network devices operating in the same band. This *out-of-network* or *extrinsic* interference will possibly be

heterogeneous as the interfering nodes may have different transmit power, density, etc. We model the extrinsic interference by considering M additional tiers of nodes, where the nodes in tier m are located according to a homogeneous PPP $\Phi_m \triangleq \{x_{i,m}, i \in \mathbb{N}\}$ of intensity λ_m, independently of other tiers. We let $\hat{P}$ and $\{\hat{P}_m\}_{m=1}^M$ denote the transmit powers of tiers Φ and $\{\Phi_m\}_{m=1}^M$ respectively. Without loss of generality, we assume the transmit powers to be normalized by $\hat{P}$ in the subsequent analysis. We use $P_m = \frac{\hat{P}_m}{\hat{P}}$ to denote the transmit power of the interfering tier Φ_m, while the transmit power of the TX tier Φ is $P = 1$.

C. Signal Model

We assume the nodes are equipped with a single antenna each and employ orthogonal frequency division multiple access (OFDMA) for communication. We consider a transmission scheme where a group of K cooperating TXs jointly transmit the same data to a given user over the same time-frequency resource block. Given the challenges associated with channel acquisition, none of the transmitting nodes are assumed to have any instantaneous channel knowledge. The considered joint transmission scheme is simple as it does not require joint encoding at the cooperating transmitters. To further reduce the coordination overhead, we do not assume any tight synchronization among the in-cluster TXs. The user, however, is required to know the composite downlink channel from the in-cluster transmitters for coherent detection. The signals transmitted by the cooperating TXs superimpose non-coherently at the receiver, resulting in a received power boost. Moreover, interference seen by the user is treated as noise for the purpose of decoding.

We now describe the channel model. Let H_i be the channel power gain for the link from a TX i in Φ to the given user. We consider a rich scattering environment where all the links experience IID narrowband Rayleigh fading such that the small-scale fading power is exponentially distributed with unit mean, i.e., $H_i \sim \exp(1)$. Leveraging Slivnyak's theorem [15], we consider a typical user located at the origin, and characterize the performance in the presence of co-channel interference and noise. Note that the timing offset between cooperating transmitters causes the received signal power to vary substantially across a large number of subcarriers within the coherence bandwidth (particularly when the timing offset and coherence bandwidth are assumed to be relatively large). Therefore, we can consider the average received power across these subcarriers for analysis (along the lines of [25]). With such a non-coherent joint transmission scheme (see [25, Appendix A] for details), the signal-to-interference-plus-noise ratio (SINR) at the user can be expressed as

$$\gamma \triangleq \frac{\sum\limits_{i=1}^{K} \mathbb{1}_i \|x_i\|^{-\eta} H_i}{I + \sigma^2} \tag{2}$$

where the Bernoulli random variable $\mathbb{1}_i$ models the uncertainty due to bursty energy arrivals at the transmitter such that $\Pr[\mathbb{1}_i = 1] = p_{\text{tr},i}$ and $\Pr[\mathbb{1}_i = 0] = 1 - p_{\text{tr},i} \triangleq q_{\text{tr},i}$ for the in-cluster TXs (i.e., $1 \le i \le K$), η denotes the pathloss exponent, while $\sigma^2 = \frac{\hat{\sigma}^2}{\hat{P}}$ where $\hat{\sigma}^2$ gives the variance of the receiver noise, which we assume to be zero-mean circularly symmetric complex Gaussian. Moreover, I denotes the aggregate interference power observed at the receiver. For analytical tractability, it is assumed that the signals transmitted by the interfering nodes superimpose non-coherently at the receiver, which would typically be the case. The aggregate interference power I can be expressed as

$$\begin{aligned} I &= I_0 + \sum_{m=1}^{M} I_m \\ &= \underbrace{\sum_{i=K+1}^{\infty} \mathbb{1}_i \|x_i\|^{-\eta} H_i}_{\text{intrinsic}} + \underbrace{\sum_{m=1}^{M} \sum_{x_{i,m} \in \Phi_m} \mathbb{1}_{i,m} P_m \|x_{i,m}\|^{-\eta} H_{i,m}}_{\text{extrinsic}} \end{aligned} \tag{3}$$

where the first term I_0 accounts for the in-network or intrinsic interference due to the out-of-cluster TXs in Φ. Here, $\Pr[\mathbb{1}_i = 1] = p_{\text{tr},o}$ while $\Pr[\mathbb{1}_i = 0] = 1 - p_{\text{tr},o} \triangleq q_{\text{tr},o}$ for all the out-of-cluster TXs (i.e., $i > K$). The second term in (3) models the extrinsic or out-of-network interference from the nodes belonging to the M interfering tiers $\{\Phi_m\}_{m=1}^M$. Note that for the interfering tiers, we use a slightly modified notation by including i, m in the subscript to denote a node i that belongs to the interfering tier Φ_m. As done for the TX tier Φ, we can similarly define $\Pr[\mathbb{1}_{i,m} = 1] = p_{\text{tr}}^{(m)}$ for the nodes in tier m. The assumptions about the channel model are as explained for the TX tier Φ, i.e., $H_{i,m} \sim \exp(1)$. From (2) and (3), it also follows that a system with powers $\hat{P}$, $\{\hat{P}_m\}_{m=1}^M$ has the same SINR as a normalized system with powers $P = 1$, $\{P_m\}_{m=1}^M$. Without loss of generality, we therefore focus on a system with normalized transmit powers.

Notation. Table I summarizes the notation introduced in this section. We adopt the following notation for the transmission probabilities of the nodes belonging to tier Φ. For $i = 1, \cdots, K$, we define $p_{\text{tr},i} \triangleq 1 - q_{\text{tr},i}$ to be the transmission probability of the i^{th} in-cluster TX belonging to Φ, whereas $p_{\text{tr},o}$ gives the transmission probability of all other (i.e., out-of-cluster) TXs in Φ. Similarly, for $m = 1, \cdots, M$, we define $p_{\text{tr}}^{(m)} \triangleq 1 - q_{\text{tr}}^{(m)}$ to be the transmission probability of the nodes belonging to the interfering tier Φ_m. The above notation allows both the in-cluster and out-of-cluster nodes to have different transmission probabilities. This is in line with the considered model, where we have allowed the nodes to have possibly different energy harvesting capabilities. For ease of exposition, we define $\Xi = \left[q_{\text{tr},1}, \cdots, q_{\text{tr},K}, q_{\text{tr},o}, q_{\text{tr}}^{(1)}, \cdots, q_{\text{tr}}^{(M)}\right]$, which depends on the energy harvesting parameters (i.e., energy harvesting rate and energy buffer size).

We now define the notation to describe the cluster geometry. For a given cluster of size K, let $\{d_i\}_{i=1}^K$ denote a realization of the respective distances between a user and its K serving TXs. This set is assumed to be arranged in ascending order such that d_1 and d_K refer to the closest and farthest serving TXs respectively. We define $\omega_i = \frac{d_i}{d_K}$ $(0 < \omega_i \le 1)$ such that $\{\omega_i\}_{i=1}^K$ denotes a set of normalized distances. The cluster geometry parameters $\{\omega_i\}_{i=1}^K$ can be physically interpreted in

TABLE I
MODEL PARAMETERS

Notation	Description
K	cluster size
η	path-loss exponent
p_{ch}	channel access probability
$p_{\text{tr}} \triangleq 1 - q_{\text{tr}}$	transmission probability
ρ	energy harvesting rate
S	energy buffer size
$\Phi_u; \lambda_u$	PPP with intensity λ_u modeling RX locations.
$\Phi; \lambda$	PPP with intensity λ modeling TX locations.
$\{p_{\text{tr},i}\}_{i=1}^{K}$	transmission probabilities of K in-cluster TXs.
$p_{\text{tr},o}$	transmission probability of out-of-cluster TXs in Φ.
$\Phi_m; \lambda_m$ $(1 \le m \le M)$	PPP with intensity λ_m modeling node locations in tier m.
$p_{\text{tr}}^{(m)}$ $(1 \le m \le M)$	transmission probability of nodes in Φ_m.
P_m $(1 \le m \le M)$	normalized transmit power of nodes in Φ_m.

terms of the interference-free guard zone around the user. For example, a smaller ω_1 corresponds to clusters having larger guard zones around receivers (and vice versa). We also define $\Omega = \{\omega_1^\eta, \cdots, \omega_K^\eta\}$ and $\hat{\Omega} = \{\frac{\omega_1^\eta}{q_{\text{tr},1}}, \cdots, \frac{\omega_K^\eta}{q_{\text{tr},K}}\}$. For generality, we allow Ω to have duplicate elements and further define the set $\{\delta_1^\eta, \cdots, \delta_\tau^\eta\}$ to consist of all the unique elements of the set Ω, where δ_i^η occurs in Ω with multiplicity n_i. Note that $\tau = 1, \cdots, K$, where $\tau = 1$ denotes the case when Ω has identical elements, whereas $\tau = K$ when Ω has distinct elements[2]. We further define $\binom{K}{K-i}_\Omega$ to be the set of all products of the elements of Ω taken $K - i$ at a time. For instance, when $K = 3$, $\binom{3}{1}_\Omega = \{\omega_1^\eta, \omega_2^\eta, \omega_3^\eta\}$, $\binom{3}{2}_\Omega = \{\omega_1^\eta\omega_2^\eta, \omega_2^\eta\omega_3^\eta, \omega_3^\eta\omega_1^\eta\}$, and $\binom{3}{3}_\Omega = \{\omega_1^\eta\omega_2^\eta\omega_3^\eta\}$. We also define a set operator $\overset{+}{\sum}[\cdot]$ that returns the sum of the elements of the set that it operates on. We further define

$$\alpha_i(\Omega) = (-1)^i \overset{+}{\sum} \left[\binom{K}{K-i}_\Omega \right]. \tag{4}$$

The summation in (4) is taken over the elements of the set $\binom{K}{K-i}_\Omega$. Similarly, the definition of $\alpha_i(\hat{\Omega})$ follows from (4) with the set Ω now replaced by $\hat{\Omega}$. For the intensity parameters, we define $\Lambda = [\lambda, \lambda_1, \cdots, \lambda_M]$ where λ gives the intensity of the PPP Φ, while $\{\lambda_m\}_{m=1}^M$ denote the same for the interfering tiers $\{\Phi_m\}_{m=1}^M$.

III. STOCHASTIC GEOMETRY ANALYSIS

In this section, we derive closed-form analytical expressions for the link success probability, the cluster access probability, and the overall success probability.

[2]Note that Ω is a multiset since it may have duplicate elements. For cleaner exposition, however, we call Ω (and other such multisets) a set in this paper.

A. Link Success Probability

In this subsection, we focus on the receivers which have been selected for service in a given resource. We provide closed-form expressions to characterize the complementary cumulative distribution function (CCDF) of the SINR γ (or alternatively the link success probability) as a function of network parameters and cluster geometry. We characterize the performance for two cases, namely the absolute cluster geometry and the average cluster geometry. While the former helps evaluate the performance of a given cluster, the latter caters to the general case where the absolute cluster geometry is averaged out.

1) Absolute cluster geometry: We first calculate the link success probability for a user for the conditional case where the absolute cluster geometry (i.e., in-cluster distances) is specified. The following theorem characterizes the link-level performance of a specific cluster amid interference and noise.

Theorem 1. For a cluster of size K, the CCDF of γ, $\bar{F}_\gamma(K, \theta) = \Pr[\gamma > \theta]$, can be tightly approximated as a function of the intensity parameters (Λ), noise power (σ^2), energy harvesting parameters (Ξ) and in-cluster distances $\left(\{d_i\}_{i=1}^K\right)$ using

$$\bar{F}_\gamma(K, \theta) \approx G \sum_{u=1}^{\tau} \sum_{v=1}^{n_u} \left(\sum_{m=0}^{K-1} \left(\alpha_m(\hat{\Omega}) - \alpha_m(\Omega) \right) \mathrm{A}_m(n_u, v) \right) \mathrm{B}_{u,v}(\theta) \tag{5}$$

where

$$G = \prod_{i=1}^{K} q_{\text{tr},i} \tag{6}$$

and

$$\mathrm{A}_m(n_u, v) = (-1)^{n_u - v} {\delta_u}^{-v\eta} \sum_{\sum_{i=1}^{\tau} k_i = n_u - v} \binom{m}{k_u} {\delta_u}^{\eta(m-k_u)} \times \prod_{j \ne u}^{\tau} \binom{n_j + k_j - 1}{k_j} \left({\delta_j}^\eta - {\delta_u}^\eta \right)^{-(n_j + k_j)}. \tag{7}$$

The summation in (7) is taken over all possible combinations of non-negative integer indices $k_1, \cdots, k_\tau$ that add up to $n_u - v$. Further,

$$\mathrm{B}_{u,v}(\theta) = \sum_{\ell=1}^{v} \binom{v}{\ell} (-1)^{\ell+1} \Delta_{u,\ell}(\theta) \tag{8}$$

where

$$\Delta_{u,\ell}(\theta) = \underbrace{e^{-\theta\kappa\ell(d_K\delta_u)^\eta\sigma^2}}_{\text{noise}} \underbrace{e^{-\pi p_{\text{tr},o}\lambda {d_K}^2 \mathcal{F}(\delta_u^\eta\theta\kappa\ell,\eta)}}_{\text{intrinsic}} \underbrace{\Psi_u(M)}_{\text{extrinsic}}, \tag{9}$$

$$\Psi_u(M) = \prod_{m=1}^{M} e^{-\pi p_{\text{tr}}^{(m)} \lambda_m {\delta_u}^2 {d_K}^2 (\theta\kappa\ell P_m)^{\frac{2}{\eta}} \Gamma\left(1+\frac{2}{\eta}\right)\Gamma\left(1-\frac{2}{\eta}\right)}, \tag{10}$$

with $\kappa = (v!)^{-\frac{1}{v}}$ and

$$\mathcal{F}(t_1, t_2) = \frac{2\,t_1}{t_2 - 2}\,{}_2F_1\left(1, 1 - \frac{2}{t_2}, 2 - \frac{2}{t_2}, -t_1\right), \quad (11)$$

where ${}_2F_1(\cdot)$ is the Gauss hypergeometric function [32], and $\Gamma(\cdot)$ is the Gamma function.

Proof. See Appendix A. ∎

The terms $\mathrm{B}_{u,v}(\cdot)$ in (5) or $\Delta_{u,\ell}(\cdot)$ in (8) capture the impact of the aggregate interference and receiver noise. In particular, the term $e^{-\theta\kappa\ell(d_K\delta_u)^\eta\sigma^2}$ in (9) is due to noise, $e^{-\pi p_{\mathrm{tr},o}\lambda {d_K}^2\mathcal{F}(\delta_u^\eta\theta\kappa\ell,\eta)}$ is due to intrinsic interference, while $\Psi_u(M)$ accounts for the extrinsic interference due to the M interfering tiers. Also note that G defined in (6) gives the probability that none of the in-cluster nodes transmit. It is a function of the energy harvesting parameters as well as the cluster size.

Remark 1. Note that Theorem 1 allows the in-cluster TXs to have possibly different energy harvesting rates or buffer sizes, and is therefore useful for getting general insights about the performance when the given cluster consists of heterogeneous TXs. Similarly, the multi-tier approach allows capturing the heterogeneity in out-of-cluster nodes. Furthermore, all the interfering TXs can be assumed to have the maximum harvesting rate/buffer size to get a lower bound on performance.

Corollary 1. $\theta \to 0$. In the low-outage regime, the performance is limited by the in-cluster energy harvesting parameters and the cluster size. In particular, as $\theta \to 0$ in (5), we get $\lim_{\theta\to 0}\bar{F}_\gamma(K,\theta) = 1 - G$, where G given in (6) defines a limit on the performance and in fact represents the exact link outage probability in the asymptotic regime. In this regime, the performance is independent of the out-of-cluster parameters. This observation also holds for Theorem 2.

Theorem 1 is indeed general as it is applicable to any given absolute cluster geometry. For instance, it allows two or more in-cluster TXs to be equidistant from the receiver. Later, numerical results confirm the accuracy of the analytical expression proposed in Theorem 1. The following proposition treats a special case of Theorem 1 where the in-cluster distances $\{d_i\}_{i=1}^K$ are assumed to be distinct (i.e., $\tau = K$). We note that an *exact* characterization of the link success probability is possible for this case.

Proposition 1. Given a cluster of size K with distinct in-cluster distances $\left(\{d_i\}_{i=1}^K\right)$, the CCDF of γ, $\bar{F}_\gamma(K,\theta) = \Pr[\gamma > \theta]$, can be expressed in terms of the intensity parameters (Λ), noise power (σ^2), and energy harvesting parameters (Ξ) as

$$\bar{F}_\gamma(K,\theta) = G\sum_{j=1}^{K}\left(\frac{\sum_{i=0}^{K-1}\left(\alpha_i(\hat{\Omega}) - \alpha_i(\Omega)\right)(\omega_j^\eta)^i}{\omega_j^\eta\left(\prod_{l\neq j}^{K}\omega_l^\eta - \omega_j^\eta\right)}\right)\mathrm{C}_j(\theta) \quad (12)$$

where G follows from (6), and

$$\mathrm{C}_j(\theta) = \underbrace{e^{-d_j^\eta\theta\sigma^2}}_{\text{noise}}\underbrace{e^{-\pi p_{\mathrm{tr},o}\lambda d_K^2\mathcal{F}\left(\omega_j^\eta\theta,\eta\right)}}_{\text{intrinsic}}\underbrace{\mathrm{D}_j(M)}_{\text{extrinsic}} \quad (13)$$

with

$$\mathrm{D}_j(M) = \prod_{m=1}^{M} e^{-\pi p_{\mathrm{tr}}^{(m)}\lambda_m d_j^2(\theta P_m)^{\frac{2}{\eta}}\Gamma\left(1+\frac{2}{\eta}\right)\Gamma\left(1-\frac{2}{\eta}\right)}. \quad (14)$$

Proof. See Appendix B. ∎

Recall that G is the link outage probability in the asymptotic regime $\theta \to 0$ (Corollary 1). As illustrated in (13), the link success probability depends on the aggregate interference and noise via the term $\mathrm{C}_j(\theta)$ only.

Corollary 2. $\{q_{\mathrm{tr},i}\}_{i=1}^K = q_{\mathrm{tr},o} \triangleq q_{\mathrm{tr}}$. When all the in-cluster TXs have identical energy harvesting capabilities, i.e., $q_{\mathrm{tr},i} = q_{\mathrm{tr},o} \triangleq q_{\mathrm{tr}}$, the CCDF in (12) simplifies to

$$\bar{F}_\gamma(K,\theta) = \sum_{j=1}^{K}\left(\frac{\sum_{i=0}^{K-1}\alpha_i(\Omega)\left({q_{\mathrm{tr}}}^i - {q_{\mathrm{tr}}}^K\right)(\omega_j^\eta)^i}{\omega_j^\eta\left(\prod_{l\neq j}^{K}\omega_l^\eta - \omega_j^\eta\right)}\right)\mathrm{C}_j(\theta) \quad (15)$$

where $\mathrm{C}_j(\theta)$ is as given in (13).

2) Average cluster geometry: We now consider the case where the in-cluster TXs are located randomly according to Φ. Recall that the TXs in Φ have identical energy harvesting capabilities such that $\{q_{\mathrm{tr},i}\}_{i=1}^K = q_{\mathrm{tr},o} \triangleq q_{\mathrm{tr}}$. The following theorem characterizes the link success probability by averaging out over the absolute in-cluster distances given the cluster geometry parameters. In other words, the following result does not correspond to a particular cluster. Rather, it is averaged over all such clusters that have the same cluster geometry parameters $\{\omega_i\}_{i=1}^K$. Also note the use of superscript $\prime$ in $\bar{F}'_\gamma(K,\theta)$ to differentiate it from the earlier notation $\bar{F}_\gamma(K,\theta)$ used in Theorem 1.

Theorem 2. In the interference-limited regime ($\sigma^2 \to 0$), the CCDF of γ, $\bar{F}'_\gamma(K,\theta)$, can be expressed as a function of the cluster size (K), the intensity parameters (Λ), and the energy harvesting parameters (Ξ) for a cluster geometry $\left(\{\omega_i\}_{i=1}^K\right)$ as

$$\bar{F}'_\gamma(K,\theta) = \sum_{j=1}^{K}\left(\frac{\sum_{i=0}^{K-1}\alpha_i(\Omega)\left({q_{\mathrm{tr}}}^i - {q_{\mathrm{tr}}}^K\right)(\omega_j^\eta)^i}{\omega_j^\eta\left(\prod_{l\neq j}^{K}\omega_l^\eta - \omega_j^\eta\right)}\right)\mathcal{V}_j(K,\theta) \quad (16)$$

where

$$\mathcal{V}_j(K,\theta) = \left(1 + \mathcal{F}\left(\omega_j^\eta\theta,\eta\right) + \Upsilon_j(M)\right)^{-K} \quad (17)$$

and

$$\Upsilon_j(M) = {\omega_j}^2 \theta^{\frac{2}{\eta}} \Gamma\left(1+\frac{2}{\eta}\right)\Gamma\left(1-\frac{2}{\eta}\right)\sum_{m=1}^{M} \tilde{p}_{\text{tr}}^{(m)} \tilde{\lambda}_m {P_m}^{\frac{2}{\eta}}. \tag{18}$$

Note that $\mathcal{F}(\cdot,\cdot)$ follows from (11), and we define $\tilde{p}_{\text{tr}}^{(m)} = \frac{p_{\text{tr}}^{(m)}}{p_{\text{tr}}}$ and $\tilde{\lambda}_m = \frac{\lambda_m}{\lambda}$.

Proof. See Appendix C. ■

Note that the term $\mathcal{V}_j(K,\theta)$ in (16) captures the impact of the aggregate interference. In particular, the term $\mathcal{F}\left(\omega_j^{\eta}\theta,\eta\right)$ in (17) is due to the intrinsic interference, while $\Upsilon_j(M)$ is due to the extrinsic interference. Further, the link success probability relates to the intensity parameters only via the term $\Upsilon_j(M)$ given in (18).

Remark 2. For the case with no extrinsic interference, i.e., with the M interfering tiers turned off, the CCDF expression in Theorem 2 is independent of the TX intensity λ. Intuitively, this is because the useful signal power tends to increase with λ (as the cluster radius tends to decrease), but so does the interference such that the two effects cancel out. This follows by observing that the link success probability depends on the intensity parameters via $\Upsilon_j(M)$ given in (18). Setting $\{P_m\}_{m=1}^{M}$ equal to 0 yields $\Upsilon_j(M)=0$, and the result follows.

Remark 3. With the M interfering tiers now turned on, the CCDF expression in Theorem 2 is no longer independent of the intensity parameters Λ. In this case, increasing the TX intensity λ (or more generally the effective intensity $p_{\text{tr}}\lambda$) helps dilute the intensity of the interfering tiers. This is supported by (18) where the term inside the summation vanishes as λ is increased. This neutralizes the harmful term $\Upsilon_j(M)$, which captures the effect of the extrinsic interference. This is in contrast to the previous case where the TX intensity λ plays no role.

The following corollaries have been obtained assuming the M interfering tiers to be turned off.

Corollary 3. $p_{\text{tr}} \to 1$. It is worth noting that without energy harvesting and a random medium access protocol, i.e., as $p_{\text{tr}} \to 1$ in (16), and further assuming the M interfering tiers to be turned off, we can retrieve the expression for the CCDF of γ in a traditionally powered cooperative network as given in [33], which Theorem 2 generalizes.

Corollary 4. $K=1$. For the non-cooperative case, the expression in (16) simplifies to $\bar{F}'_{\gamma}(1,\theta) = (1-q_{\text{tr}})(1+\mathcal{F}(\theta,\eta))^{-1}$. As $p_{\text{tr}} \to 0$, $\bar{F}'_{\gamma}(1,\theta) \to 0$, which shows that the energy harvesting parameters are critical in determining outage. Furthermore, with $q_{\text{tr}}=0$, we can retrieve the CCDF expression for the signal-to-interference ratio (SIR) in a traditionally powered non-cooperative network as given in [19].

Corollary 5. $S \to \infty$. As the energy buffer size S goes to infinity, the transmission probability p_{tr} approaches $\min(\rho, p_{\text{ch}})$ [12]. Plugging $q_{\text{tr}} = 1-\min(\rho,p_{\text{ch}})$ in (16) yields the outage probability floor as the buffer size goes to infinity for a given outage threshold θ and cluster size K. For example, for $\rho < p_{\text{ch}}$, the outage probability floor is given by

$$P'_{\text{out},S\to\infty}(K,\theta) = 1-\sum_{j=1}^{K}\left(\frac{\sum_{i=0}^{K-1}\alpha_i(\Omega)\left((1-\rho)^i-(1-\rho)^K\right)(\omega_j^{\eta})^i}{\omega_j^{\eta}\left(\prod_{l\neq j}^{K}\omega_l^{\eta}-\omega_j^{\eta}\right)}\right)\mathcal{V}_j(K,\theta) \tag{19}$$

where $\mathcal{V}_j(K,\theta)$ is as given in (17). Furthermore, as $\theta \to 0$, $\lim_{\theta\to 0} P'_{\text{out},S\to\infty}(K,\theta) = (1-\rho)^K$. This defines the minimum possible outage probability floor for a given energy harvesting rate ρ and cluster size K in the large energy buffer regime.

Corollary 6. $\rho > p_{\text{ch}}$. As the energy harvesting rate ρ exceeds the channel access probability p_{ch}, the transmission probability $p_{\text{tr}} \to p_{\text{ch}}$ assuming a sufficiently large energy buffer, i.e., as $S \to \infty$. In this regime, the network is independent of the energy harvesting parameters and behaves like a traditionally-powered network. The outage probability expression for this regime can be obtained similar to Corollary 5.

These results shows that the proposed analytical framework is fairly general with the traditionally-powered cooperative and non-cooperative networks as special cases. Note that this subsection provided an analytical treatment of the link success probability at receivers that have already been selected for service. To pave the way for the overall performance metric, the next subsection treats the case where the receivers compete for cluster access, and characterizes the cluster access probability at a typical receiver.

B. Cluster Access Probability

There could be multiple candidate users competing over one or more TXs of a cluster. In each slot, only one such user will be selected uniformly at random to be served by its desired cluster. We define the cluster access probability $p_{\text{clus}}(K,\beta)$ as the probability that a random user is granted access to the desired cluster, i.e., it is selected for service in a cluster comprising its K closest TXs. We also note that $p_{\text{clus}}(K,\beta)$ is a geometric quantity that is completely characterized by (i) the cluster size K and (ii) the ratio of the transmitter and receiver densities β. Since the exact analytical characterization seems challenging, we propose simple closed-form expressions to approximate the cluster access probability. We illustrate this point by considering the simple non-cooperative case $K=1$, where each user is served only by its closest TX. In this case, a typical user will be selected for service with a probability $1/n$ given that there are n candidate users for the typical TX. Therefore, $p_{\text{clus}}(K,\beta) = \sum_{n=1}^{\infty}\frac{1}{n}\Pr[n \text{ candidate users}]$. Note that for $K=1$, $\Pr[n \text{ candidate users}]$ corresponds to the probability of having n users within the typical Voronoi cell. While the exact area distribution of a Voronoi cell is not known, several analytical approximations exist in the literature [34]. Such an approximation was used to characterize the user distribution in a Voronoi cell [35]. Leveraging the results in

[34], [35] for the probability distribution of the number of users in a cell, the cluster access probability for the non-cooperative case can be approximated as

$$p_{\text{clus}}(K=1,\beta) \approx \sum_{i=1}^{\infty} \frac{3.5^{3.5}}{i!} \frac{\Gamma(i+3.5)}{\Gamma(3.5)} \left(\frac{1}{\beta}\right)^{i-1} \left(3.5+\frac{1}{\beta}\right)^{-(i+3.5)} \tag{20}$$

where $\beta = \frac{p_{\text{tr}}\lambda}{\lambda_u}$ is the transmitter receiver density ratio, as $p_{\text{tr}}\lambda$ is the density of the transmitter PPP obtained by an independent thinning of Φ, while λ_u is the density of the receiver PPP Φ_u. Though this approach yields an analytical expression for $p_{\text{clus}}(K,\beta)$ for the non-cooperative case $K=1$, the extension of this formulation to the cooperative case $K>1$ is rather challenging.

Proposed Approximation: We now propose an analytical approximation for the cluster access probability $p_{\text{clus}}(K,\beta)$ for the general case. The proposed approach is based on the following observation. When a user does not have any neighboring users within a certain guard radius, its desired set of TXs is less likely to be conflicted by other users. This means that the user is more likely to be selected for service by its desired cluster. The guard radius, in turn, depends on the cluster size K as well the density ratio β. We, therefore, calculate the probability that a user has no neighbors within the specified guard zone, and the guard zone is expressed as a function of the cluster size and the density ratio. For a typical user in Φ_u located at the origin, recall that $\|x_K\|$ denotes the random distance to its Kth closest transmitter in Φ. Similarly, we let y_1 be the random distance to its closest neighboring user in Φ_u. We can interpret $p_{\text{clus}}(K,\beta)$ as the probability that there is no other user within a radius $c\times\|x_K\|$ of the typical user, i.e., $p_{\text{clus}} = \Pr[y_1 > c\|x_K\|]$. The constant $c>0$ controls the radius of this guard zone around the user. Consider

$$\mathbb{E}\left[\Pr\left[y_1 > c\|x_K\| \middle| \|x_K\|\right]\right] \overset{(a)}{=} \mathbb{E}[e^{-\lambda_u \pi c^2 \|x_K\|^2}] \overset{(b)}{=} \left[1+c^2\frac{\lambda_u}{p_{\text{tr}}\lambda}\right]^{-K} \tag{21}$$

where (a) follows by calculating the void probability for Φ_u in a ball of radius $c\|x_K\|$, while (b) is obtained by averaging over $\|x_K\|$, which follows a generalized Gamma distribution [36]. Note that we have not yet characterized c in terms of the model parameters. We propose setting $c=\sqrt{\frac{C_1(K)}{1+C_2(K)\frac{\lambda_u}{p_{\text{tr}}\lambda}}}$ in (21), where $C_1(K)$ and $C_2(K)$ are functions of K. This results in the following analytical approximation

$$p_{\text{clus}}(K,\beta) \approx \frac{1}{\left[1+\frac{C_1(K)}{\beta+C_2(K)}\right]^K}. \tag{22}$$

Note that $p_{\text{clus}}(K,\beta)$ is a function of the cluster size K and the density ratio β. Using basic curve fitting tools, we found that the linear expressions $C_1(K)=0.06K+0.78$ and $C_2(K)=0.34K-0.49$ result in a good fit for the simulation-based $p_{\text{clus}}(K,\beta)$ over the considered range of $1<K<6$ (see Fig. 7). While this range is sufficient for the setup considered in this paper, similar curve-fitting approach may be used to obtain a numerical fit for larger cluster sizes. For the non-cooperative case $K=1$, we found that $C_1(K)=0.725$ and $C_2(K)=0$ give an accurate fit. Also, the proposed expression $\left[1+\frac{0.725}{\beta}\right]^{-1}$ is much simpler than the analytical approximation given in (20) for $K=1$. The proposed approximation for $p_{\text{clus}}(K,\beta)$ is validated in Fig. 7.

Remark 4. The cluster access probability increases with the density ratio and decreases with the cluster size. This is because for a given cluster size, a higher density ratio suggests that the typical user requires a relatively smaller user-free guard zone, which increases the cluster access probability. For a given density ratio, a larger cluster size causes more receivers to compete for the same cluster, reducing the cluster access probability. Moreover, the cluster access probability also increases with the energy harvesting rate and the buffer size since the density ratio is proportional to the transmission probability.

C. Overall Success Probability

We now introduce an overall performance metric to characterize the joint impact of the link success probability and the cluster access probability. We define the overall success probability $P_{\text{suc}}(\cdot)$ as the joint probability that a user is selected for service and the transmission that follows results in a successful packet reception, i.e., $P_{\text{suc}}(K,\theta) = \Pr\left[\gamma>\theta, \frac{y_1}{\|x_K\|}>c\right]$, where we have used the notation from Section III-B. Note that these two events are not independent as both depend on the same underlying geometry. Leveraging the framework developed in Section III-A and III-B, we provide a closed-form expression for $P_{\text{suc}}(\cdot)$ in terms of the model parameters.

Theorem 3. The overall success probability $P_{\text{suc}}(K,\theta)$ can be expressed as a function of the cluster size (K), the intensity parameters (Λ,λ_u), and the energy harvesting parameters (Ξ) for a cluster geometry $\left(\{\omega_i\}_{i=1}^K\right)$ as

$$P_{\text{suc}}(K,\theta) \approx \sum_{j=1}^{K} \left(\frac{\sum_{i=0}^{K-1} \alpha_i(\Omega)\left({q_{\text{tr}}}^i - {q_{\text{tr}}}^K\right)(\omega_j^\eta)^i}{\omega_j^\eta\left(\prod_{l\neq j}^{K}\omega_l^\eta - \omega_j^\eta\right)} \right) \mathcal{Z}_j(K,\theta) \tag{23}$$

where

$$\mathcal{Z}_j(K,\theta) = \left(1+\mathcal{F}\left(\omega_j^\eta\theta,\eta\right)+\Upsilon_j(M)+\frac{C_1(K)}{\beta+C_2(K)}\right)^{-K}, \tag{24}$$

$\mathcal{F}(\cdot,\cdot)$ and $\Upsilon_j(\cdot)$ are given in (11) and (18), $C_1(K)$ and $C_2(K)$ follow from (22), and $\beta=\frac{p_{\text{tr}}\lambda}{\lambda_u}$ is the density ratio.

Proof. See Appendix D. ∎

The term $\mathcal{Z}_j(K,\theta)$ in Theorem 3 incorporates the impact of the aggregate interference as well as that of the user competition over potential clusters. In particular, $\mathcal{F}\left(\omega_j^\eta\theta,\eta\right)$ in (24) is due to the intrinsic interference, $\Upsilon_j(M)$ is due

to the extrinsic interference, and $\frac{C_1(K)}{\beta+C_2(K)}$ captures the user competition for cluster access.

Remark 5. The overall success probability given in Theorem 3 also depends on the user density λ_u via the density ratio $\beta = \frac{p_{\text{tr}}\lambda}{\lambda_u}$. Moreover, even in the absence of extrinsic interference, the overall success probability still depends on the density ratio β. This is unlike Theorem 2, where the link success probability is independent of the intensity parameters when the M interfering tiers are turned off (Remark 2). This further suggests that densifying the TX tier helps improve the overall performance regardless of the presence of extrinsic interference.

Remark 6. As the density ratio β increases, the overall success probability in Theorem 3 converges to the link success probability given in Theorem 2. This is because the cluster access probability approaches unity when the density ratio is large. Therefore, the overall success probability is mainly limited by the link-level performance when the density ratio is large.

Corollary 7. $\theta \to 0$. In the low outage regime, the overall success probability is limited by the energy harvesting parameters, the cluster size as well as the density ratio β. As $\theta \to 0$ in (23), $\lim_{\theta\to 0} P_{\text{suc}}(K,\theta) = p_{\text{clus}}(K,\beta)\,(1-G)$, where G is given in (6) and $p_{\text{clus}}(K,\beta)$ follows from (22).

Remark 7. In the asymptotic regime $\theta \to 0$, we get fundamentally different insights on node cooperation for self-powered and traditionally-powered networks when $p_{\text{ch}} = 1$. In traditionally-powered networks, Corollary 7 implies that cooperation is in fact detrimental for the overall success probability, i.e., when $p_{\text{tr}} \to 1$, $G \to 0$ such that $\lim_{\theta\to 0} P_{\text{suc}}(K,\theta) = p_{\text{clus}}(K,\beta)$, which decreases as the cluster size K is increased. To see this, note that $p_{\text{clus}}(K,\beta)$ in (22) admits a simpler approximation $p_{\text{clus}}(K,\beta) \approx 1 - \frac{K}{\beta}$ when β is sufficiently large. For a self-powered network, however, the gain due to cooperation captured by the term $(1-G) = (1-{q_{\text{tr}}}^K)$ more than compensates for the loss due to $p_{\text{clus}}(K,\beta)$ when β is sufficiently large. This suggests that cooperation helps improve the overall performance in an energy harvesting network. Furthermore, due to the underlying tradeoff between the link reliability and the fraction of receivers getting served, there is an optimal cluster size that maximizes the asymptotic success probability for a given β. This analytical insight is confirmed by the numerical results presented in next section.

IV. Simulation Results

In this section, we use Monte Carlo simulations to validate the analytical results for the link success probability, the cluster access probability, and the overall success probability under different network scenarios. We also investigate the impact of several parameters such as cluster size, energy harvesting rate, and energy buffer size on the system performance to derive intuition on the system operations.

Each simulation trial consists of generating the transmitter/receiver PPPs in a finite window, according to their respective intensities. We assume that the energy arrival process at the TXs has reached its steady state. Whether or not a transmitter transmits is simulated using a Bernoulli random variable generated according to the specified energy harvesting parameters. All the wireless links are assumed to be Rayleigh fading with a path-loss exponent η. The performance metrics are computed by averaging over 10,000 such trials.

A. Link Success Probability

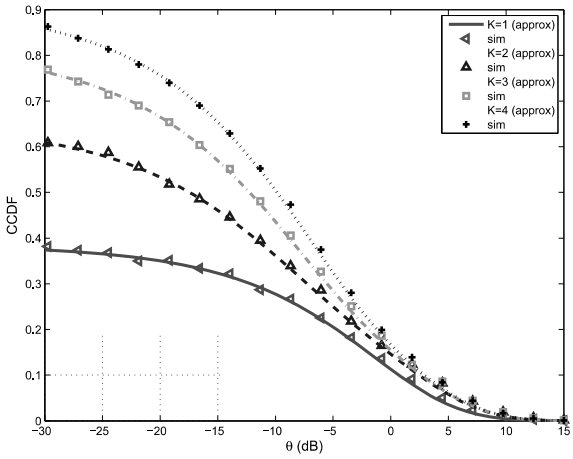

Fig. 2. CCDF of γ for various values of K given $p_{\text{ch}} = 0.7, \lambda = 0.01, \eta = 4$, $\sigma^2 = -114$ dBm, and $\{\|x_i\|\}_{i=1}^4 = \{5, 10, 10, 10\}$. The plot is obtained for a single interfering tier $M = 1$ with $\lambda_1 = 0.01$, $p_{\text{tr}}^{(1)} = 0.53$ and $P_1 = 2$. Energy harvesting parameters for the TX tier are $\{\rho_i\}_{i=1}^4 = \{0.4, 0.45, 0.5, 0.55\}$, $\rho_o = 0.55$ and $S = 2$. Simulation (sim) results agree with the analytical approximation (approx) based on Theorem 1.

1) Absolute Cluster Geometry: We first evaluate the link success probability for a specified cluster with possibly heterogeneous in-cluster TXs. This is the case treated in Theorem 1 and Proposition 1. In Fig. 2, we plot the link success probability $\bar{F}_\gamma(K,\theta)$ for various values of the cluster size K. The plot includes the curves obtained using the analytical approximation (approx) based on Theorem 1. It also includes the results obtained by Monte Carlo simulations (sim) for the specified set of parameters. The analytical model is validated since there is a complete agreement between the analytical and simulation results. Similarly, in Fig. 3, we consider the case where the in-cluster TXs have distinct link distances. It can be observed that the simulation results match completely with the (exact) analytical (anlt) results based on Proposition 1.

We can draw two conclusions from Fig. 2 and 3. First, the SINR distribution at the receiver improves with the cluster size K due to a received power boost. Second, the link outage performance is limited by the energy harvesting capabilities as the CCDF converges to $1-G$ in the low-outage regime ($\theta \to 0$) for any given cluster. This corroborates the analytical insights provided in Corollary 1.

2) Average Cluster Geometry: We now consider the case treated in Theorem 2, where the in-cluster TX locations are random. Further, all the TXs have identical energy harvesting capabilities. In Fig. 4a and 4b, we plot $\bar{F}'_\gamma(K,\theta)$, the CCDF of γ with the absolute in-cluster distances averaged out. Fig. 4a is obtained with the interfering tiers turned off, whereas

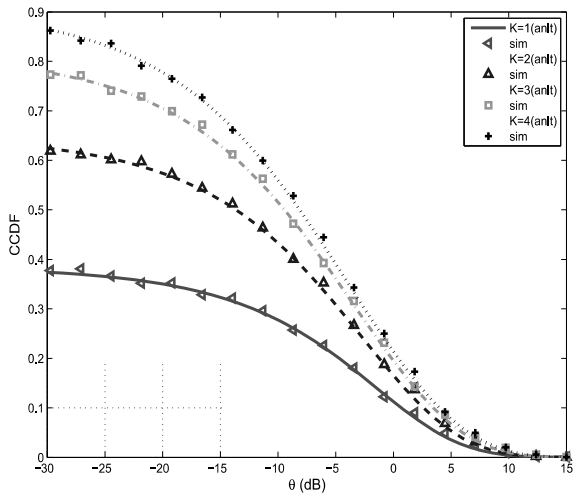

Fig. 3. CCDF of γ for various values of K given a distinct cluster geometry $\{\|x_i\|\}_{i=1}^{4}=\{5,7,9,11\}$. Other simulation parameters are same as in Fig. 2. Simulation (sim) results agree with the analytical (anlt) results based on Proposition 1.

Fig. 4b is obtained with the interfering tiers turned on. We observe a complete match between the analytical curve based on Theorem 2 and the simulated CCDF obtained via Monte Carlo simulations. Similarly, Fig. 5 shows that increasing the density of the TX tier helps improve the link performance in the presence of extrinsic interference. This also confirms the analytical insights provided in Remarks 2 and 3.

We next study how the energy harvesting parameters limit the outage performance.

3) Impact of Energy Buffer Size on Performance: We first consider how the link outage probability varies as a function of the energy buffer size. To get general performance insights, we use the asymptotic outage probability $P_{\text{out}}^{\text{as}} \triangleq G$, which defines an upper limit on performance given the energy harvesting parameters and cluster size. Note that similar insights can be obtained if the analysis is particularized for a given outage threshold θ using (16). In Fig. 6a, the asymptotic outage probability $P_{\text{out}}^{\text{as}}$ is plotted against the energy buffer size S (in log scale) for various values of the cluster size K. We see that outage can be considerably reduced by increasing the buffer size until a limit, beyond which the curves tend to flatten out. The existence of this outage probability floor follows from Corollary 5, and the floor value is specified by (19). It appears that appreciable performance gains can be extracted with a relatively small buffer size. Moreover, the benefits of having a high-capacity energy buffer tend to increase with the cluster size as depicted by the increasing steepness of the slopes (when S is small) as K is increased. This interplay between cluster and buffer sizes also suggests that the extent of cooperation could influence the design of energy harvesting devices, even though the energy harvesting process is assumed to be independent across the cooperating TXs. In addition, we observe that the outage is reduced by roughly an order of magnitude with every addition in the cluster size.

4) Impact of Energy Harvesting Rate on Performance: In Fig. 6b, the asymptotic outage probability $P_{\text{out}}^{\text{as}}$ is plotted against the energy harvesting rate ρ for various values of energy buffer size S. We observe that outage reduces with the increase in energy harvesting rate at the transmitters. Moreover, using a larger energy buffer brings about further reduction in outage due to enhanced energy availability at the transmitters. Furthermore, the gains from using a larger buffer size are more evident at relatively high energy harvesting rates. Fig. 6b also corroborates the previous observation (cf. Fig. 6a) that substantial performance can be extracted by using a relatively small buffer size. For example, $S = 10$ suffices for this setup. In addition, if the energy harvesting rate ρ exceeds the channel access probability p_{ch}, and the buffer size is allowed to increase, the outage performance limit becomes independent of the energy harvesting rate ρ. For example, this behavior is evident in Fig. 6b for $S = 100$. This is because under these conditions, the energy harvesting system tends to behave like a traditionally powered system. This is consistent with Corollary 6.

B. Cluster Access Probability

We now validate the analytical approximation for the cluster access probability $p_{\text{clus}}(K,\beta)$ proposed in (22). In each simulation trial, the transmitter/receiver PPPs are (independently) generated in a finite window according to the specified densities. When there is no conflict, a receiver is assigned to its K closest TXs. In case of multiple candidate receivers, only one is randomly selected for service. The cluster access probability is calculated by averaging over 10,000 such trials. In Fig. 7, there is a nice agreement between analytical and Monte Carlo simulation-based results. Moreover, in line with Corollary 7, $p_{\text{clus}}(K,\beta)$ decreases with the cluster size K and increases with the density ratio β.

C. Overall Success Probability

The overall success probability is plotted in Fig. 8. The plots shows that cooperation is generally beneficial for the overall success probability in self-powered networks (unlike the traditional case as discussed in Remark 7). Moreover, it also captures the underlying tension between two competing metrics, the link performance and the fraction of receivers getting served. As explained in Remark 7, this leads to an optimal cluster size that maximizes the overall network-wide performance. We further observe that the optimal cluster size increases with the density ratio due to an underlying increase in the cluster access probability. Though the plot is obtained for the asymptotic case $\theta \to 0$, similar trends can be observed when the analysis is particularized for a given value of θ.

V. Conclusions

We have considered a large-scale cooperative wireless network where clusters of self-powered transmitters jointly serve a desired receiver. Using stochastic geometry, we have provided a tractable analytical framework to characterize the link and network-level performance at the receiver amid heterogeneous network interference. The analysis leads to several useful insights on system operation. First, the overall success

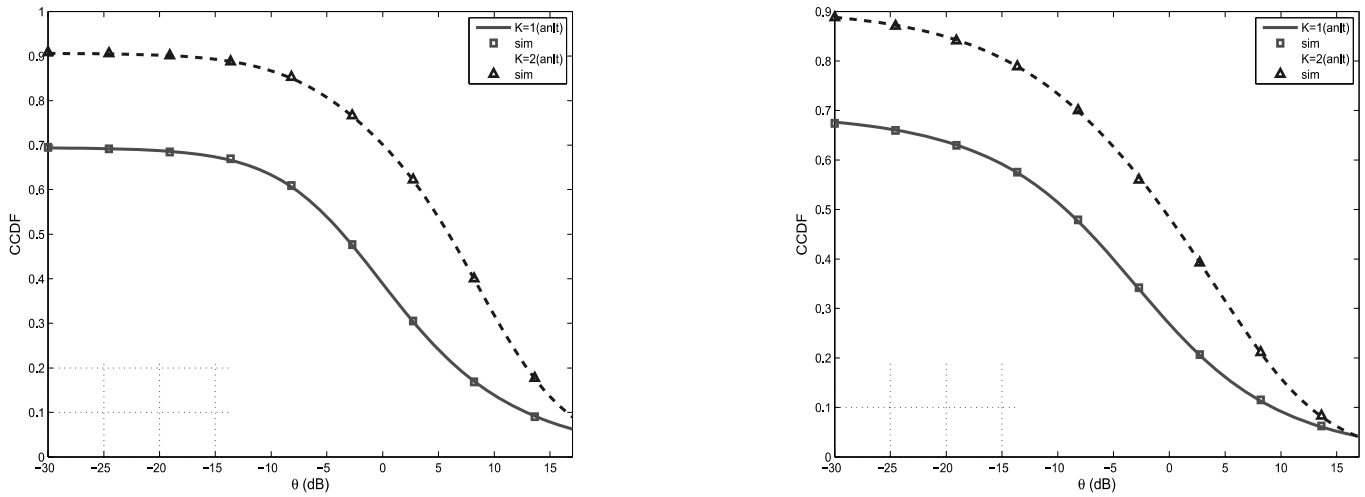

Fig. 4. (a) CCDF of γ in the interference-limited regime for $K \in \{1, 2\}$ with the M tiers turned off (i.e., intrinsic interference only). The plot includes the analytical (anlt) curve based on Theorem 2 as well as the simulated (sim) CCDF of γ. The simulation parameters are $\omega_1 = 1$ for $K = 1$ and $\{\omega_i\}_{i=1}^2 = \{0.5, 1\}$ for $K = 2$, $p_{\text{ch}} = 0.8$ and $\eta = 4$. The energy harvesting parameters are $\rho = 0.75$ and $S = 2$ for all TXs. (b) For the same parameters, CCDF of γ is plotted when both intrinsic and extrinsic interference are present. Other parameters include $M = 1$, $P_1 = 2$, and $p_{\text{tr}}^{(1)} = 0.5$. Unlike (a) which is independent of intensity, (b) is obtained for $\lambda = 0.1$ and $\lambda_1 = 0.05$.

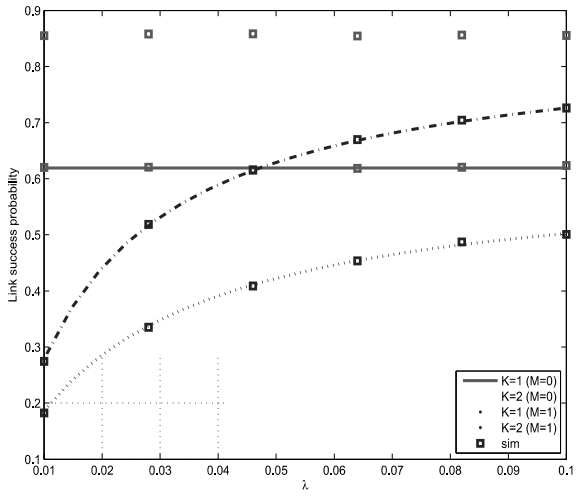

Fig. 5. The link success probability vs. the TX density λ with and without extrinsic interference. Densifying the TX tier helps improve performance in the presence of extrinsic interference ($M > 1$). The simulation parameters are $\theta = 0.1$, $\omega_1 = 1$ for $K = 1$ and $\{\omega_i\}_{i=1}^2 = \{0.5, 1\}$ for $K = 2$, $p_{\text{ch}} = 0.8$ and $\eta = 3.6$. The energy harvesting parameters are $\rho = 0.75$ and $S = 2$ for all TXs. The parameters for extrinsic interference are $M = 1$, $P_1 = 2$, and $p_{\text{tr}}^{(1)} = 0.5$.

probability might degrade when the cluster size is too large, unlike the link success probability which improves with the cluster size. This is due to the underlying tradeoff between the link quality and the fraction of receivers getting served. Moreover, the resulting optimal cluster size increases with the density ratio due to the underlying improvement in the cluster access probability. Second, we get fundamentally different insights on node cooperation in self-powered and traditionally-powered networks. In particular, in the asymptotic regime where the link outage threshold is small, it is optimal not to cooperate in a traditionally-powered network. In a self-powered network, however, cooperation could be beneficial since it helps overcome the performance loss due to uncertain energy availability at the transmitter. Third, the overall performance improves with the buffer size and the energy harvesting rate. Furthermore, most performance gains can be extracted using a relatively small buffer size, with the improvement becoming more pronounced for large clusters in sufficiently dense networks.

Appendix A: Derivation of Theorem 1

We first state a lemma that will be used in the following derivation.

Lemma 2. For a non-negative integer n, and a positive real number x, the regularized upper incomplete Gamma function $\mathcal{Q}(n, x)$ can be upper bounded as $\mathcal{Q}(n, x) \leq 1 - (1 - e^{-cx})^n$, where $c = (n!)^{-\frac{1}{n}}$.

Proof. See [37]. ∎

For ease of exposition, we use an alternative notation for the nodes in TX tier Φ from here on. Specifically, the subscript 0 is used while referring to the quantities of nodes in the TX tier, e.g., $\Phi_0 = \Phi$, $\lambda_0 = \lambda$, $x_{i,m} = x_i$. Using (2), we write $\bar{F}_\gamma(K, \theta) = \Pr[\gamma > \theta] = \mathbb{E}\left[\Pr\left[S_K > \theta d_K{}^\eta \left(I + \sigma^2\right)\right]\right]$, where $S_K = \sum_{i=1}^{K} \mathbb{1}_i \hat{H}_i$ and $\hat{H}_i = H_i \omega_i^{-\eta}$. We condition on the in-cluster distances such that $\|x_i\| = d_i$ for $i = 1, \cdots, K$. To proceed further, we first find the CCDF of S_K, where S_K is a sum of K independent random variables. Note that $\hat{H}_i$ is exponentially distributed with mean $\omega_i^{-\eta}$, whereas the indicator $\mathbb{1}_i$ follows a Bernoulli distribution with mean $p_{\text{tr},i}$,

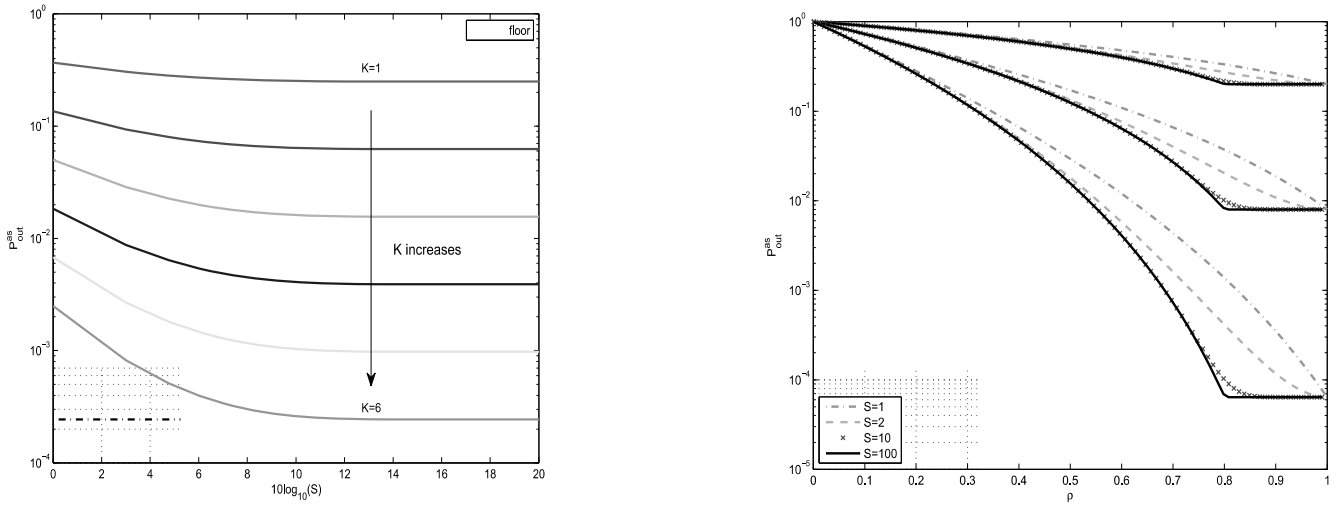

(a) (b)

Fig. 6. (a) Impact of energy buffer size S on asymptotic outage probability $P_{\text{out}}^{\text{as}}$ for various values of K at fixed $\rho = 0.75$ and $p_{\text{ch}} = 0.8$. The outage probability floor is based on Corollary 5. The utility of having a larger energy buffer increases with the cluster size. (b) Impact of energy harvesting rate ρ on asymptotic outage probability $P_{\text{out}}^{\text{as}}$ for various values of energy buffer size S at fixed $p_{\text{ch}} = 0.8$. The curves are plotted for cluster size $K \in \{1, 3, 6\}$. The outage performance becomes independent of the energy harvesting rate as the latter exceeds the channel access probability for sufficiently large energy buffers.

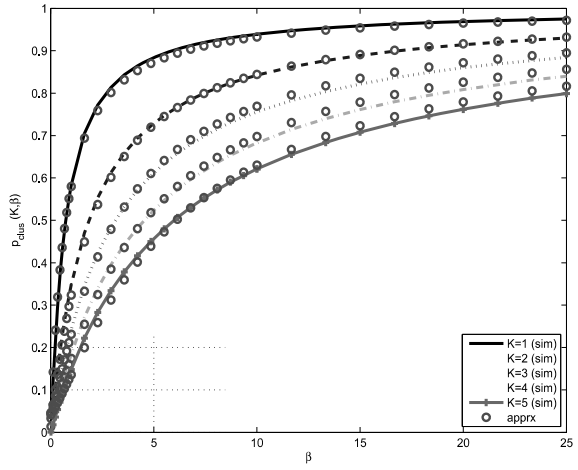

Fig. 7. Cluster access probability $p_{\text{clus}}(K, \beta)$ as a function of density ratio β for different values of the cluster size K. The results based on analytical approximation (apprx) in (22) closely match the simulation (sim) results. $p_{\text{clus}}(K, \beta)$ also gives the overall success probability for a traditionally-powered network in the low outage regime ($\theta \to 0$). The results are in line with Remark 4 and 5.

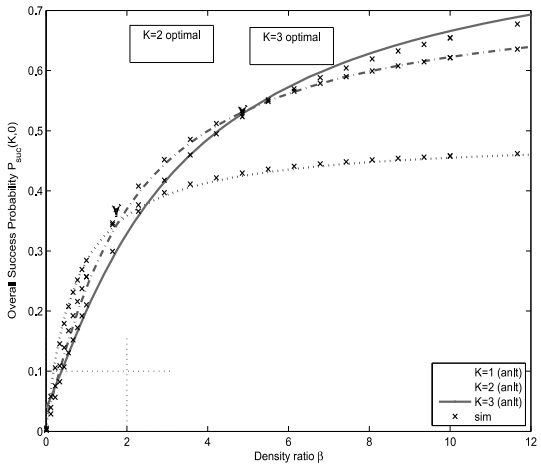

Fig. 8. Overall success probability $P_{\text{suc}}(K, \theta)$ in the asymptotic regime ($\theta \to 0$) as a function of the density ratio β for different values of the cluster size K. Cooperation improves performance in a self-powered network. There is an optimal cluster size K for a given value of β. The energy harvesting parameters are fixed to $S = 2$ and $\rho = 0.5$, and $p_{\text{ch}} = 0.8$.

independently of $\hat{H}_i$. The CCDF of S_K can be expressed as ($x \geq 0$)

$$\bar{F}_{S_k}(x) = G \sum_{u=1}^{\tau} \sum_{v=1}^{n_u} \left(\sum_{m=0}^{K-1} \left(\alpha_m(\hat{\Omega}) - \alpha_m(\Omega) \right) \mathrm{A}_m(n_u, v) \right) \mathcal{Q}(v, \delta_u^{\eta} x) \tag{A.1}$$

where $\mathrm{A}_m(n_u, v)$ is given by (7), while $\mathcal{Q}(a, b) = \frac{1}{\Gamma(a)} \int_b^{\infty} t^{a-1} e^{-t} \mathrm{d}t$ denotes the regularized upper incomplete Gamma function. The expression in (A.1) can be obtained by finding the characteristic function of S_K, applying partial fraction expansion and then taking the inverse transform [38]. Conditioning on the aggregate interference power I, we can write $\bar{F}_{\gamma|I}(K, \theta) = \bar{F}_{S_K}\left(\theta {d_K}^{\eta} (I + \sigma^2)\right)$. Using (A.1), and by unconditioning with respect to I, $\bar{F}_{\gamma}(K, \theta)$ can be expressed as (for $\theta \geq 0$)

$$\bar{F}_{\gamma}(K, \theta) = G \sum_{u=1}^{\tau} \sum_{v=1}^{n_u} \left(\sum_{m=0}^{K-1} \left(\alpha_m(\hat{\Omega}) - \alpha_m(\Omega) \right) \mathrm{A}_m(n_u, v) \right) \times \mathbb{E}\left[\mathcal{Q}\left(v, \delta_u^{\eta} {d_K}^{\eta} \theta \left(I + \sigma^2 \right) \right) \right] \tag{A.2}$$

where the expectation in (A.2) is over the aggregate interference power I, i.e., over both fading and interferer locations. A series expansion of the incomplete Gamma function gives the following alternative form

$$\mathbb{E}\left[\mathcal{Q}\left(v, \delta_u^{\eta} {d_K}^{\eta}\theta\left(I+\sigma^2\right)\right)\right] = \sum_{i=0}^{v-1} e^{-\delta_u^{\eta}{d_K}^{\eta}\theta\sigma^2}\mathbb{E}\left[e^{-\delta_u^{\eta}{d_K}^{\eta}\theta I}\frac{\left(\delta_u^{\eta}{d_K}^{\eta}\theta\left(I+\sigma^2\right)\right)^i}{i!}\right]. \tag{A.3}$$

To avoid directly dealing with the expectation in (A.3), which seems rather unwieldy, we leverage the upper bound for $\mathcal{Q}\left(\cdot,\cdot\right)$ given in Lemma 2.

$$\begin{aligned}\mathbb{E}&\left[\mathcal{Q}\left(v, \delta_u^{\eta} {d_K}^{\eta}\theta\left(I+\sigma^2\right)\right)\right]\\ &\leq \mathbb{E}\left[1-\left(1-e^{-\kappa\delta_u^{\eta}{d_K}^{\eta}\theta\left(I+\sigma^2\right)}\right)^v\right]\\ &= \mathbb{E}\left[\sum_{\ell=1}^{v}\binom{v}{\ell}(-1)^{\ell+1}e^{-\kappa\ell\delta_u^{\eta}{d_K}^{\eta}\theta\left(I+\sigma^2\right)}\right]\\ &= \sum_{\ell=1}^{v}\binom{v}{\ell}(-1)^{\ell+1}e^{-\kappa\ell\delta_u^{\eta}{d_K}^{\eta}\theta\sigma^2}\mathbb{E}\left[e^{-\kappa\ell\delta_u^{\eta}{d_K}^{\eta}\theta I}\right] \end{aligned}\tag{A.4}$$

where $\kappa = (v!)^{-\frac{1}{v}}$, and the last equation follows by applying the Binomial theorem. The next step is to evaluate the expectation $\mathbb{E}\left[e^{-\kappa\ell\delta_u^{\eta}{d_K}^{\eta}\theta I}\right]$. Since the PPPs $\{\Phi_m\}_{m=0}^{M}$ are assumed to be independent, it follows that

$$\mathbb{E}\left[e^{-\kappa\ell\delta_u^{\eta}{d_K}^{\eta}\theta I}\right] = \mathbb{E}\left[e^{\kappa\ell\delta_u^{\eta}{d_K}^{\eta}\theta I_0}\right]\prod_{m=1}^{M}\mathbb{E}\left[e^{-\kappa\ell\delta_u^{\eta}{d_K}^{\eta}\theta I_m}\right] \tag{A.5}$$

where the first term (with $m=0$) corresponds to intrinsic interference, whereas the remaining terms ($m\geq 1$) correspond to extrinsic interference. The expectation in (A.5) can be evaluated using the Laplace transform of I_m, which we denote by $\mathcal{L}_{I_m}(s) = \mathbb{E}\left[e^{-sI_m}\right]$.

$$\begin{aligned}\mathcal{L}_{I_m}(s) &= \mathbb{E}\left[e^{-s\left(\sum\limits_{x_{i,m}\in\Phi_m\setminus\mathcal{B}(g_m)} P_m\mathbb{1}_i H_i\|x_{i,m}\|^{-\eta}\right)}\right]\\ &\overset{(a)}{=} \mathbb{E}\left[\prod_{x_{i,m}\in\hat{\Phi}_m\setminus\mathcal{B}(g_m)}\mathrm{E}\left[e^{-sP_mH_i\|x_{i,m}\|^{-\eta}}\right]\right]\\ &\overset{(b)}{=} \mathbb{E}\left[\prod_{x_{i,m}\in\hat{\Phi}_m\setminus\mathcal{B}(g_m)}\frac{1}{1+sP_m{x_{i,m}}^{-\eta}}\right]\\ &= \exp\left(-2\pi\hat{\lambda}_m\int_{g_m}^{\infty}\frac{x}{1+s^{-1}{P_m}^{-1}x^{\eta}}\mathrm{d}x\right)\end{aligned}\tag{A.6}$$

where $\mathcal{B}(g_m)$ denotes a disc of radius g_m centered at the origin, and models an interference-free guard zone around the user with respect to tier m. The inner expectation in (a) is over fading power while the outer expectation is over the PPP Φ_m of intensity λ_m outside the guard zone $\mathcal{B}(g_m)$. Next, we exploit the property of independent thinning of a PPP to deal with the transmission indicator and consider a (thinned) PPP $\hat{\Phi}_m$ with effective density $\hat{\lambda}_m = p_{\mathrm{tr}}^{(m)}\lambda_m$ for $1\leq m\leq M$ and $\hat{\lambda}_m = p_{\mathrm{tr},o}\lambda_m$ for $m=0$. As the fading is IID across links and from further conditioning over the location, we obtain (b). The last equation follows by invoking the probability generating functional (PGFL) [15] of the PPP and by further algebraic manipulations. With some additional algebraic steps, (A.6) can be expressed in terms of a hypergeometric function, which with $s = \kappa\ell\delta_u^{\eta}{d_K}^{\eta}\theta$ gives

$$\mathcal{L}_{I_m}(s)|_{s=\kappa\ell\delta_u^{\eta}{d_K}^{\eta}\theta} = \exp\left(-\pi\hat{\lambda}_m g_m^2\mathcal{F}\left(\frac{\delta_u^{\eta}{d_K}^{\eta}}{g_m^{\eta}}P_m\kappa\ell\theta,\eta\right)\right) \tag{A.7}$$

where $\mathcal{F}(\cdot,\cdot)$ is given by (11). To compute the expectation of the term in (A.5) arising due to the out-of-cluster TXs in Φ_0, set $g_0 = d_K$. This is because the cluster is assumed to consist of the K closest nodes, and the interference is due to the nodes located outside this protection zone. For the interfering tiers $\{\Phi_m\}_{m=1}^{M}$, however, no such protection zone is assumed. Without an interferer-free protection zone (i.e., $g_m\to 0$), $\mathcal{L}_{I_m}(s)$ further simplifies to

$$\mathcal{L}_{I_m}(s)|_{s=\kappa\ell\delta_u^{\eta}{d_K}^{\eta}\theta} = \exp\left(-\pi\hat{\lambda}_m{\delta_u}^2{d_K}^2\Gamma(1+2/\eta)\Gamma(1-2/\eta)(P_m\theta\kappa\ell)^{2/\eta}\right). \tag{A.8}$$

Evaluating the expectation in (A.2) using (A.7), (A.8), and further substituting $P_0=1$, $\hat{\lambda}_0 = p_{\mathrm{tr},o}\lambda_0$, and $\hat{\lambda}_m = p_{\mathrm{tr}}^{(m)}\lambda_m$, we obtain the result in Theorem 1.

Appendix B: Derivation of Proposition 1

Similar to Appendix A, we can express $\bar{F}_{\gamma}\left(K,\theta\right) = \mathbb{E}\left[\Pr\left[S_K>\theta\|x_K\|^{\eta}\left(I+\sigma^2\right)\right]\right]$, where $S_K = \sum\limits_{i=1}^{K}\mathbb{1}_i\hat{H}_i$, and $\hat{H}_i = H_i\omega_i^{-\eta}$. Further, we condition on the in-cluster distances such that $\|x_i\| = d_i$ for $i\in\{1,\cdots,K\}$. Recall that Proposition 1 is specialized to the case where the set Ω consists of distinct elements (i.e., $\tau = K$). Given a distinct cluster geometry, the CCDF of S_K given in (A.1) can be further simplified to the following form (for $x\geq 0$)

$$\bar{F}_{S_k}\left(x\right) = G\sum_{j=1}^{K}\left(\frac{\sum\limits_{i=0}^{K-1}\left(\alpha_i(\hat{\Omega})-\alpha_i(\Omega)\right)(\omega_j^{\eta})^i}{\omega_j^{\eta}\left(\prod\limits_{l\neq j}^{K}\omega_l^{\eta}-\omega_j^{\eta}\right)}\right)e^{-\omega_j^{\eta}x} \tag{B.1}$$

where (B.1) follows by plugging $\tau=K$ and $n_u=1$ (for $u=1,\cdots,\tau$) in (A.1). Conditioning on the aggregate interference power I, we can write $\bar{F}_{\gamma|I}\left(K,\theta\right) = \bar{F}_{S_K}\left(\theta{d_K}^{\eta}(I+\sigma^2)\right)$. Using (B.1), and taking expectation with respect to I, we can

$$\mathbb{E}_{d_K}\left[\mathrm{C}_j(\theta)\right] = \int_{r>0} e^{-\pi p_{\mathrm{tr}}\lambda r^2 \mathcal{F}\left(\omega_j^{\eta}\theta,\eta\right)} \prod_{m=1}^{M} e^{-\pi p_{\mathrm{tr}}^{(m)}\lambda_m {\omega_j}^2 (P_m\theta)^{\frac{2}{\eta}}\Gamma\left(1+\frac{2}{\eta}\right)\Gamma\left(1-\frac{2}{\eta}\right)} \frac{2\left(p_{\mathrm{tr}}\lambda\pi r^2\right)^K e^{-p_{\mathrm{tr}}\lambda\pi r^2}}{r\Gamma(K)}\mathrm{d}r$$
$$= \int_0^{\infty} \frac{e^{-\upsilon}\upsilon^{K-1}}{\Gamma(K)\left(1+\mathcal{F}\left(\omega_j^{\eta}\theta,\eta\right)+{\omega_j}^2\theta^{\frac{2}{\eta}}\Gamma\left(1+\frac{2}{\eta}\right)\Gamma\left(1-\frac{2}{\eta}\right)\sum_{m=1}^{M}\tilde{p}_{\mathrm{tr}}^{(m)}\tilde{\lambda}_m {P_m}^{\frac{2}{\eta}}\right)^K}\mathrm{d}\upsilon$$
$$= \frac{1}{\left(1+\mathcal{F}\left(\omega_j^{\eta}\theta,\eta\right)+{\omega_j}^2\theta^{\frac{2}{\eta}}\Gamma\left(1+\frac{2}{\eta}\right)\Gamma\left(1-\frac{2}{\eta}\right)\sum_{m=1}^{M}\tilde{p}_{\mathrm{tr}}^{(m)}\tilde{\lambda}_m {P_m}^{\frac{2}{\eta}}\right)^K} \tag{C.2}$$

$$\upsilon = \pi r^2\left(p_{\mathrm{tr}}\lambda\left(1+\mathcal{F}\left(\omega_j^{\eta}\theta,\eta\right)\right)+{\omega_j}^2\theta^{\frac{2}{\eta}}\Gamma\left(1+\frac{2}{\eta}\right)\Gamma\left(1-\frac{2}{\eta}\right)\sum_{m=1}^{M}\tilde{p}_{\mathrm{tr}}^{(m)}\tilde{\lambda}_m {P_m}^{\frac{2}{\eta}}\right) \tag{C.3}$$

express $\bar{F}_{\gamma}\left(K,\theta\right)$ (for $\theta \geq 0$) as

$$\bar{F}_{\gamma}(K,\theta) = G\sum_{j=1}^{K}\left(\frac{\sum_{i=0}^{K-1}\left(\alpha_i(\hat{\Omega})-\alpha_i(\Omega)\right)\left(\omega_j^{\eta}\right)^i}{\omega_j^{\eta}\left(\prod_{l\neq j}^{K}\omega_l^{\eta}-\omega_j^{\eta}\right)}\right)\mathbb{E}\left[e^{-\omega_j^{\eta}{d_K}^{\eta}\theta\left(I+\sigma^2\right)}\right] \tag{B.2}$$

where the expectation in (B.2) is over the aggregate interference power I. Unlike Appendix A where an approximation was used, the expectation in (B.2) can be directly evaluated using (A.6). Since the PPPs are assumed to be independent, it follows that

$$\mathbb{E}\left[e^{-{d_j}^{\eta}\theta I}\right] = \mathbb{E}\left[e^{-d_j^{\eta}\theta I_0}\right]\prod_{m=1}^{M}\mathbb{E}\left[e^{-d_j^{\eta}\theta I_m}\right]. \tag{B.3}$$

As the rest of the derivation follows directly from Appendix A, some steps are omitted. Evaluating (A.6) at $s = d_j^{\eta}\theta$ yields

$$\mathcal{L}_{I_m}(s)|_{s=d_j^{\eta}\theta} = \exp\left(-\pi\hat{\lambda}_m g_m^2 \mathcal{F}\left(\frac{d_j^{\eta}}{g_m^{\eta}}P_m\theta,\eta\right)\right). \tag{B.4}$$

Note that we use an alternative notation for the nodes in TX tier, e.g., $\Phi_0 = \Phi$, $\lambda_0 = \lambda$. To compute the expectation of the term in (B.3) arising due to intrinsic interferers in Φ_0, set $g_0 = d_K$ in (B.4). Similarly, for the interfering tiers $\{\Phi_m\}_{m=1}^{M}$, the expectation in (B.3) is given by

$$\mathcal{L}_{I_m}(s)|_{s=d_j^{\eta}\theta} = \exp\left(-\pi\hat{\lambda}_m {d_j}^2\Gamma(1+2/\eta)\Gamma(1-2/\eta)(P_m\theta)^{2/\eta}\right). \tag{B.5}$$

Evaluating the expectation in (B.2) using (B.4), (B.5), and further substituting $P_0 = 1$, $\hat{\lambda}_0 = p_{\mathrm{tr},o}\lambda_0$, $\hat{\lambda}_m = p_{\mathrm{tr}}^{(m)}\lambda_m$ and $d_j = \omega_j d_K$, yields the result in Proposition 1.

Appendix C: Derivation of Theorem 2

We begin the proof along the lines of [33] by leveraging a known result on the PPP distance distribution. As shown in [36], the distance $\|x_K\|$, between a typical user and its Kth closest TX, follows a generalized Gamma distribution, i.e.,

$$f_{\|x_K\|}(r) = \frac{2}{r\Gamma(K)}\left(p_{\mathrm{tr}}\lambda\pi r^2\right)^K e^{-p_{\mathrm{tr}}\lambda\pi r^2}. \tag{C.1}$$

Plugging $\sigma^2 = 0$ in (13), and unconditioning the distance d_K according to the distribution of $\|x_K\|$, we arrive at the expression in (C.2) (given at the top of the page) where the last equation is obtained by using a dummy variable (given in (C.3)) for integration, and using the definition of the Gamma function $\Gamma(K) = \int_0^{\infty} e^{-x}x^{K-1}\mathrm{d}x$. Unconditioning (15) with respect to d_K, and using (C.2), we recover the expression in Theorem 2.

Appendix D: Derivation of Theorem 3

Leveraging the notation from Section III-B, we define $P_{\mathrm{suc}}\left(K,\theta\right) = \Pr\left[\gamma > \theta, y_1 > c\|x_K\|\right] = \mathbb{E}\left[\Pr\left[\gamma > \theta, y_1 > c\|x_K\|\big|\|x_K\|\right]\right] = \mathbb{E}\left[\Pr\left[\gamma > \theta\big|\|x_K\|\right]\Pr\left[y_1 > c\|x_K\|\big|\|x_K\|\right]\right]$, where the expectation is with respect to the distance $\|x_K\|$. Note that $\Pr\left[\gamma > \theta\big|\|x_K\|\right]$ follows from (13) with $\sigma^2 \to 0$, while $\Pr\left[y_1 > c\|x_K\|\big|\|x_K\|\right] = e^{-\lambda_u\pi c^2\|x_K\|^2}$. Following steps similar to those in Appendix C, and using the approximation $c = \sqrt{\frac{C_1(K)}{1+C_2(K)/\beta}}$ proposed in Section III-B, we retrieve the expression in Theorem 3.

References

[1] T. Khan, P. Orlik, and K. J. Kim, "A stochastic geometry analysis of cooperative wireless networks powered by energy harvesting," in *2015 IEEE Int. Conf. Commun. (ICC)*, Jun. 2015, pp. 1988–1993.

[2] S. Ulukus, A. Yener, E. Erkip, O. Simeone, M. Zorzi, P. Grover, and K. Huang, "Energy harvesting wireless communications: A review of recent advances," *IEEE J. Sel. Areas Commun.*, vol. 33, no. 3, pp. 360–381, Mar. 2015.

[3] M. Gorlatova, J. Sarik, G. Grebla, M. Cong, I. Kymissis, and G. Zussman, "Movers and shakers: Kinetic energy harvesting for the internet of things," *IEEE J. Sel. Areas Commun.*, vol. 33, no. 8, pp. 1624–1639, Aug. 2015.

[4] H. Dhillon, Y. Li, P. Nuggehalli, Z. Pi, and J. Andrews, "Fundamentals of heterogeneous cellular networks with energy harvesting," *IEEE Trans. Wireless Commun.*, vol. 13, no. 5, pp. 2782–2797, May 2014.

[5] A. Zanella *et al.*, "Internet of things for smart cities," *IEEE Internet Things J.*, vol. 1, no. 1, pp. 22–32, Feb. 2014.

[6] S. Sudevalayam and P. Kulkarni, "Energy harvesting sensor nodes: Survey and implications," *IEEE Commun. Surveys Tuts.*, vol. 13, no. 3, pp. 443–461, Third 2011.

[7] D. Gunduz, K. Stamatiou, N. Michelusi, and M. Zorzi, "Designing intelligent energy harvesting communication systems," *IEEE Commun. Mag.*, vol. 52, no. 1, pp. 210–216, Jan. 2014.

[8] O. Ozel, K. Tutuncuoglu, J. Yang, S. Ulukus, and A. Yener, "Transmission with energy harvesting nodes in fading wireless channels: Optimal policies," *IEEE J. Sel. Areas Commun.*, vol. 29, no. 8, pp. 1732–1743, Sep. 2011.

[9] C. K. Ho and R. Zhang, "Optimal energy allocation for wireless communications with energy harvesting constraints," *IEEE Tran. Sig. Proc.*, vol. 60, no. 9, pp. 4808–4818, Sep. 2012.

[10] K. Tutuncuoglu and A. Yener, "Sum-rate optimal power policies for energy harvesting transmitters in an interference channel," *Journal of Communications and Networks*, vol. 14, no. 2, pp. 151–161, Apr. 2012.

[11] M. Antepli, E. Uysal-Biyikoglu, and H. Erkal, "Optimal packet scheduling on an energy harvesting broadcast link," *IEEE J. Sel. Areas Commun.*, vol. 29, no. 8, pp. 1721–1731, Sep. 2011.

[12] K. Huang, "Spatial throughput of mobile ad hoc networks powered by energy harvesting," *IEEE Trans. Inf. Theory*, vol. 59, no. 11, pp. 7597–7612, Nov. 2013.

[13] R. Vaze, "Transmission capacity of wireless ad hoc networks with energy harvesting nodes," in *IEEE Global Conf. on Sig. and Inf. Proc.*, Dec. 2013, pp. 353–358.

[14] S. Lee *et al.*, "Opportunistic wireless energy harvesting in cognitive radio networks," *IEEE Trans. Wireless Commun.*, vol. 12, no. 9, pp. 4788–4799, Sep. 2013.

[15] M. Haenggi, *Stochastic geometry for wireless networks*. Cambridge University Press, 2012.

[16] F. Baccelli, B. Blaszczyszyn, and P. Muhlethaler, "An Aloha protocol for multihop mobile wireless networks," *IEEE Trans. Inf. Theory*, vol. 52, no. 2, pp. 421–436, Feb. 2006.

[17] S. Weber, J. Andrews, and N. Jindal, "An overview of the transmission capacity of wireless networks," *IEEE Trans. Commun.*, vol. 58, no. 12, pp. 3593–3604, Dec. 2010.

[18] H. ElSawy, E. Hossain, and M. Haenggi, "Stochastic geometry for modeling, analysis, and design of multi-tier and cognitive cellular wireless networks: A survey," *IEEE Commun. Surveys Tuts.*, vol. 15, no. 3, pp. 996–1019, Jul. 2013.

[19] J. Andrews, F. Baccelli, and R. Ganti, "A tractable approach to coverage and rate in cellular networks," *IEEE Trans. Commun.*, vol. 59, no. 11, pp. 3122–3134, Nov. 2011.

[20] H. S. Dhillon, R. K. Ganti, F. Baccelli, and J. G. Andrews, "Modeling and analysis of K-tier downlink heterogeneous cellular networks," *IEEE J. Sel. Areas Commun.*, vol. 30, no. 3, pp. 550–560, Apr. 2012.

[21] N. Lee, D. Morales-Jimenez, A. Lozano, and R. Heath, "Spectral efficiency of dynamic coordinated beamforming: A stochastic geometry approach," *IEEE Trans. Wireless Commun.*, vol. 14, no. 1, pp. 230–241, Jan. 2015.

[22] S. Akoum and R. W. Heath, "Interference coordination: Random clustering and adaptive limited feedback," *IEEE Trans. Sig. Proc.*, vol. 61, no. 5-8, pp. 1822–1834, Apr. 2013.

[23] F. Baccelli and A. Giovanidis, "A stochastic geometry framework for analyzing pairwise-cooperative cellular networks," *IEEE Trans. Wireless Commun.*, vol. PP, no. 99, pp. 1–1, 2014.

[24] G. Nigam, P. Minero, and M. Haenggi, "Coordinated multipoint in heterogeneous networks: A stochastic geometry approach," in *IEEE Globecom Workshops*. IEEE, 2013, pp. 145–150.

[25] R. Tanbourgi, S. Singh, J. G. Andrews, and F. K. Jondral, "A tractable model for non-coherent joint-transmission base station cooperation," *arXiv preprint arXiv:1308.0041*, 2013.

[26] K. Huang and V. Lau, "Enabling wireless power transfer in cellular networks: Architecture, modeling and deployment," *IEEE Trans. Wireless Commun.*, vol. 13, no. 2, pp. 902–912, Feb. 2014.

[27] T. A. Khan, A. Alkhateeb, and R. W. Heath, "Millimeter wave energy harvesting," *IEEE Trans. Wireless Commun.*, vol. 15, no. 9, pp. 6048–6062, Sep. 2016.

[28] I. Krikidis, "Simultaneous information and energy transfer in large-scale networks with/without relaying," *IEEE Trans. Commun.*, vol. 62, no. 3, pp. 900–912, Mar. 2014.

[29] Z. Ding, I. Krikidis, B. Sharif, and H. V. Poor, "Wireless information and power transfer in cooperative networks with spatially random relays," *IEEE Trans. Wireless Commun.*, vol. 13, no. 8, pp. 4440–4453, Aug. 2014.

[30] J. Jeon and A. Ephremides, "On the stability of random multiple access with stochastic energy harvesting," *IEEE J. Sel. Areas Commun.*, vol. 33, no. 3, pp. 571–584, Mar. 2015.

[31] A. M. Ibrahim, O. Ercetin, and T. ElBatt, "Stability analysis of slotted aloha with opportunistic RF energy harvesting," *arXiv preprint arXiv:1501.06954*, 2015.

[32] G. Gasper and M. Rahman, *Basic hypergeometric series*. Cambridge University Press, 2004, vol. 96.

[33] N. Lee, R. W. Heath, D. Morales-Jimenez, and A. Lozano, "Base station cooperation with dynamic clustering in super-dense cloud-RAN," in *IEEE Globecom Workshops*, Dec. 2013, pp. 784–788.

[34] J.-S. Ferenc and Z. Nda, "On the size distribution of poisson voronoi cells," *Physica A: Statistical Mechanics and its Applications*, vol. 385, no. 2, pp. 518 – 526, 2007. [Online]. Available: http://www.sciencedirect.com/science/article/pii/S0378437107007546

[35] S. Singh, H. Dhillon, and J. Andrews, "Offloading in heterogeneous networks: Modeling, analysis, and design insights," *IEEE Trans. Wireless Commun.*, vol. 12, no. 5, pp. 2484–2497, May 2013.

[36] M. Haenggi, "On distances in uniformly random networks," *IEEE Trans. Inf. Theory*, vol. 51, no. 10, pp. 3584–3586, Oct. 2005.

[37] H. Alzer, "On some inequalities for the incomplete gamma function," *Mathematics of Computation of the American Mathematical Society*, vol. 66, no. 218, pp. 771–778, 1997.

[38] T. Khan, P. Orlik, K. J. Kim, and R. Heath, "Performance analysis of cooperative wireless networks with unreliable backhaul links," *IEEE Commun. Lett.*, vol. 19, no. 8, pp. 1386–1389, Aug. 2015.

Talha Ahmed Khan (S'10) graduated with a B.Sc. in electrical engineering from University of Engineering and Technology Lahore, Pakistan. He received the M.S.E. degree in electrical and computer engineering from The University of Texas at Austin, where he is currently working towards his Ph.D. degree. His research interests include wireless communications, stochastic geometry applications, millimeter wave communications, and energy harvesting. His industry-related research experience includes internships with Broadcom (2013), Mitsubishi Electric Research Labs (2014), and Connectivity Lab, Facebook (2016)..

Philip V. Orlik (SM'97) was born in New York, NY in 1972. He received the B.E. degree in 1994 and the M.S. degree in 1997 both from the State University of New York at Stony Brook. In 1999 he earned his Ph. D. in electrical engineering also from SUNY Stony Brook.

In 2000 he joined Mitsubishi Electric Research Laboratories Inc. located in Cambridge, MA where he is currently the Team Leader of the Mobile Systems Group. His primary research focus is on advanced wireless and mobile communications, sensor networks, ad hoc networking and UWB. Other research interests include vehicular/car-to-car communications, mobility modeling, performance analysis, and queuing theory.

Kyeong Jin Kim (SM'11) received the M.S. degree from the Korea Advanced Institute of Science and Technology (KAIST) in 1991 and the M.S. and Ph.D. degrees in electrical and computer engineering from the University of California, Santa Barbara in 2000. During 1991-1995, he was a research engineer at the video research center of Daewoo Electronics, Ltd., Korea. In 1997, he joined the data transmission and networking laboratory, University of California, Santa Barbara. After receiving his degrees, he joined the Nokia research center (NRC) and Nokia Inc., Dallas, TX, as a senior research engineer, where he was, from 2005 to 2009, an L1 specialist. During 2010-2011, he was an Invited Professor at Inha University, Korea. Since 2012, he works as a senior principal research staff in the Mitsubishi Electric Research Laboratories (MERL), Cambridge, MA. His research has been focused on the transceiver design, resource management, scheduling in the cooperative wireless communications systems, cooperative spectrum sharing system, physical layer secrecy system, and device-to-device communications.

Dr. Kim served as an editor for the IEEE COMMUNICATIONS LETTERS and serves as an editor for INTERNATIONAL JOURNAL OF ANTENNAS AND PROPAGATION. He also served as guest editors for the EURASIP JOURNAL ON WIRELESS COMMUNICATIONS AND NETWORKING: Special Issue on "Cooperative Cognitive Networks" and IET COMMUNICATIONS: Special Issue on "Secure Physical Layer Communications". Since 2013, he has served as a TPC chair for the IEEE GLOBECOM Workshop on Trusted Communications with Physical Layer Security.

Robert W. Heath Jr. (S'96 - M'01 - SM'06 - F'11) received the B.S. and M.S. degrees from the University of Virginia, Charlottesville, VA, in 1996 and 1997 respectively, and the Ph.D. from Stanford University, Stanford, CA, in 2002, all in electrical engineering. From 1998 to 2001, he was a Senior Member of the Technical Staff then a Senior Consultant at Iospan Wireless Inc, San Jose, CA where he worked on the design and implementation of the physical and link layers of the first commercial MIMO-OFDM communication system. Since January 2002, he has been with the Department of Electrical and Computer Engineering at The University of Texas at Austin where he is a Cullen Trust for Higher Education Endowed Professor, and is a Member of the Wireless Networking and Communications Group. He is also President and CEO of MIMO Wireless Inc. and Chief Innovation Officer at Kuma Signals LLC. He is a co-author of the book Millimeter Wave Wireless Communications published by Prentice Hall in 2014.

Dr. Heath has been a co-author of several best paper award recipients including recently the 2010 and 2013 EURASIP Journal on Wireless Communications and Networking best paper awards, the 2012 Signal Processing Magazine best paper award, a 2013 Signal Processing Society best paper award, 2014 EURASIP Journal on Advances in Signal Processing best paper award, and the 2014 Journal of Communications and Networks best paper award, the 2016 IEEE Communications Society Fred W. Ellersick Prize, and the 2016 IEEE Communications and Information Theory Societies Joint Paper Award. He is an ISI Highly Cited Researcher. He is also an elected member of the Board of Governors for the IEEE Signal Processing Society, a licensed Amateur Radio Operator, and a registered Professional Engineer in Texas.

Kentaro Sawa received B.E. and M.E. degrees in communications engineering from Tohoku University, Sendai, Japan, in 2002 and 2004, respectively. He joined Mitsubishi Electric Corporation, Japan, in 2004. He has been engaged in research on wireless communication systems. His current research interests include wireless communication and networking, and protocol design.